
BAYESIAN JOINT ADDITIVE FACTOR MODELS FOR MULTIVIEW LEARNING

Niccolo Anceschi

Department of Statistical Science
Duke University
Durham, NC 27708, USA
niccolo.anceschi@duke.edu

Federico Ferrari

Biostatistics and Research Decision Sciences
Merck & Co., Inc.
Rahway, NJ 07065, USA
federico.ferrari@merck.com

David B. Dunson*

Department of Statistical Science
Duke University
Durham, NC 27708, USA
dunson@duke.edu

Himel Mallick*

Division of Biostatistics, Department of Population Health Sciences
Weill Cornell Medicine, Cornell University
New York, NY 10065, USA
him4004@med.cornell.edu

ABSTRACT

It is increasingly common in a wide variety of applied settings to collect data of multiple different types on the same set of samples. Our particular focus in this article is on studying relationships between such multiview features and responses. A motivating application arises in the context of precision medicine where multi-omics data are collected to correlate with clinical outcomes. It is of interest to infer dependence within and across views while combining multimodal information to improve the prediction of outcomes. The signal-to-noise ratio can vary substantially across views, motivating more nuanced statistical tools beyond standard late and early fusion. This challenge comes with the need to preserve interpretability, select features, and obtain accurate uncertainty quantification. We propose a Joint Additive Factor Regression model (JAFAR) with a structured additive design, accounting for shared and view-specific components. We ensure identifiability via a novel dependent cumulative shrinkage process (D-CUSP) prior. We provide an efficient implementation via a partially collapsed Gibbs sampler and extend our approach to allow flexible feature and outcome distributions. Prediction of time-to-labor onset from immunome, metabolome, and proteome data illustrates performance gains against state-of-the-art competitors. Our open-source software (R package) is available at <https://github.com/niccoloanceschi/jafar>.

Keywords Bayesian inference · Multiview data integration · Factor analysis · Identifiability · Latent variables · Precision medicine

1 Introduction

In personalized medicine, it is common to gather vastly different kinds of complementary biological data by simultaneously measuring multiple assays in the same subjects, ranging across the genome, epigenome, transcriptome, proteome, and metabolome (Stelzer et al. 2021, Ding et al. 2022). Integrative analyses

*Co-corresponding authors

that combine information across such data views can deliver more comprehensive insights into patient heterogeneity and the underlying pathways dictating health outcomes (Mallick et al. 2024). Similar setups arise in diverse scientific contexts including wearable devices, electronic health records, and finance, among others (Lee & Yoo 2020, Li et al. 2021, McNaboe et al. 2022), where there is enormous potential to integrate the concurrent information from distinct vantage points to better understand between-view associations and improve prediction of outcomes.

Multiview datasets have specific characteristics that complicate their analyses: (i) they are often high-dimensional, noisy, and heterogeneous, with confounding effects unique to each layer (e.g., platform-specific batch effects); (ii) sample sizes are often very limited, particularly in clinical applications; and (iii) signal-to-noise ratios can vary substantially across views, which must be accounted for in the analysis to avoid poor results. Many methods face difficulties in identifying the predictive signal since it is common for most of the variability in the multiview features to be unrelated to the response (Carvalho et al. 2008). Our primary motivation in this article is thus to enable accurate and interpretable outcome prediction while allowing inferences on within- and across-view dependence structures. By selecting important latent variables within and across views, we aim to improve interpretability and reduce the burden of future data collection efforts by focusing measurements on response-relevant variables.

Carefully structured factor models that infer low-dimensional joint- and view-specific sources of variation are particularly promising. Early contributions in this space focused on the unsupervised paradigm (Lock et al. 2013, Li & Jung 2017, Argelaguet et al. 2018). Two-step approaches exploiting the learned factorization often fail to identify subtle response-relevant factors, leading to subpar predictive accuracy (Samorodnitsky et al. 2024). More recent contributions considered integrative factorizations in a supervised setting (Palzer et al. 2022, Li & Li 2022, Samorodnitsky et al. 2024). Although some of these contributions attempt to provide dependence-aware formulations, crucial identifiability issues of shared and view-specific latent factors are left unaddressed, harming interpretability, stability, and predictive accuracy. Alternative approaches focusing on prediction accuracy include Cooperative Learning (Ding et al. 2022) and IntegratedLearner (Mallick et al. 2024). Both these methods combine the usual squared-error loss-based predictions with a suitable machine-learning algorithm. However, by conditioning on the multiview features, neither approach allows inferences on or exploits information from inter- and intra-view correlations. One typical consequence of this is a tendency for unstable and unreliable feature selection, as from a predictive standpoint, it is sufficient to select any one of a highly correlated set of features.

To address these gaps, we propose combining a carefully designed joint additive factor regression (JAFAR) model with a novel prior process (D-CUSP) on the loading matrices from the shared component. The latter generalizes the cumulative shrinkage process prior (CUSP) (Legramanti et al. 2020) to introduce dependence among the loadings for different views and ensure identifiability of shared and view-specific components. Extending the approach of Moran et al. (2021) to the multiview case, we further allow the responses to load only on shared factors. This facilitates the identification of response-relevant sources of variability while also leading to computational and mixing improvements. Inclusion of view-specific latent factors preserves model flexibility, enabling the capture of variation unique to individual data modalities. This is particularly useful for isolating artifacts or confounding influences that may stem from modality-specific measurement instruments, thus enhancing the robustness of shared signal identification. We develop a partially collapsed Gibbs sampler (Park & van Dyk 2009) that benefits from the marginalization of view-specific factors, and we propose a modification of the *Varimax* step in *MatchAlign* (Poworoznek et al. 2021) to preserve the composite structure in shared loadings when solving rotational ambiguity. JAFAR is validated using both simulation studies and real data analysis, where it outperforms published methods in estimation and prediction.

The remainder of the paper is organized as follows. The proposed methodology is presented in detail in Section 2 focusing on an initial Gaussian specification, while flexible semiparametric extensions are detailed in the Appendix. In Section 3, we focus on simulation studies to validate the performances of JAFAR against state-of-the-art competitors. The empirical studies from Section 4 further showcase the benefits of our contribution on real data. An open-source implementation of JAFAR is available through R package *jafar*.

2 Joint Additive Factor Regression (JAFAR)

To address all the aforementioned challenges and deliver accurate response prediction from multiview data, we developed the following joint additive factor regression model

$$\begin{aligned}\mathbf{x}_{mi} &= \boldsymbol{\mu}_m + \boldsymbol{\Lambda}_m \boldsymbol{\eta}_i + \boldsymbol{\Gamma}_m \boldsymbol{\phi}_{mi} + \boldsymbol{\epsilon}_{mi} \\ y_i &= \mu_y + \boldsymbol{\theta}^\top \boldsymbol{\eta}_i + e_i.\end{aligned}\tag{1}$$

Here $\mathbf{x}_{mi} \in \mathbb{R}^{p_m}$ and $y_i \in \mathbb{R}$ represent the multiview data and the response, respectively, for each observation $i \in \{1, \dots, n\}$ and modality $m \in \{1, \dots, M\}$, where n and M are the total number of subjects and views, respectively. $\boldsymbol{\Lambda}_m \in \mathbb{R}^{p_m \times K}$ and $\boldsymbol{\Gamma}_m \in \mathbb{R}^{p_m \times K_m}$ are loadings matrices associated with K shared and $\{K_m\}_{m=1}^M$ view-specific latent factors, $\boldsymbol{\eta}_i \in \mathbb{R}^K$ and $\boldsymbol{\phi}_{mi} \in \mathbb{R}^{K_m}$. $\boldsymbol{\theta} \in \mathbb{R}^K$ is a set of factor regression coefficients connecting the response to the shared latent factors, complemented by an offset term $\mu_y \in \mathbb{R}$. The residual components e_i and $\boldsymbol{\epsilon}_{mi}$ are assumed to follow normal distributions $\mathcal{N}(0, \sigma_y^2)$ and $\mathcal{N}_{p_m}(\mathbf{0}_{p_m}, \text{diag}(\boldsymbol{\sigma}_m^2))$, with $\boldsymbol{\sigma}_m^2 = \{\sigma_{mj}^2\}_{j=1}^{p_m}$. Here \mathcal{N} and \mathcal{N}_p represent the univariate and p -variate Gaussian distributions.

The shared factors $\boldsymbol{\eta}_i$ are designated to impact at least two data components, either two covariate views or one view and the response. Conversely, the local factors $\{\boldsymbol{\phi}_{mi}\}_{m=1}^M$ aim at capturing view-specific variability unrelated to the response or different modalities, analogously to Moran et al. (2021). Other than being more suited to capture modality-specific effects or artifacts, this modeling choice is greatly advantageous in enforcing identifiability and improving mixing. In fact, all additive latent-factor formulations suffer from a specific form of non-identifiability (Chandra, Dunson & Xu 2023), beyond the typical ones of regular factor models, such as rotational ambiguity or columns and sign switching (Poworoznek et al. 2021). This is because shared factors have more descriptive power than view-specific ones and, unless constrained otherwise, there would a tendency is to use some columns of $\boldsymbol{\eta}$ to explain sources of variation related to a single view.

2.0.1 Non-identifiability of Additive Factor Models

To illustrate this, notice that the inter- and intra-view covariances induced by JAFAR by marginalizing out the latent factors are

$$\text{cov}(\mathbf{x}_{mi}) = \boldsymbol{\Lambda}_m \boldsymbol{\Lambda}_m^\top + \boldsymbol{\Gamma}_m \boldsymbol{\Gamma}_m^\top + \text{diag}(\boldsymbol{\sigma}_m^2), \quad \text{cov}(\mathbf{x}_m, \mathbf{x}_{m'}) = \boldsymbol{\Lambda}_m \boldsymbol{\Lambda}_{m'}^\top.\tag{2}$$

Concatenating all views into $\mathbf{x}_i = [\mathbf{x}_{1i}^\top, \dots, \mathbf{x}_{Mi}^\top]^\top$, this entails that the view-specific components $\boldsymbol{\Gamma}_m$ affect only the block-diagonal element of the induced covariance. In principle, JAFAR could be reformulated by dropping all view-specific components in favor of a unique set of sparse loadings matrices $\tilde{\boldsymbol{\Lambda}}_m$, shared factors $\tilde{\boldsymbol{\eta}}_i$ and sparse regression coefficients $\tilde{\boldsymbol{\theta}}$

$$\begin{aligned}\tilde{\boldsymbol{\Lambda}}_m &= [\boldsymbol{\Lambda}_m, \mathbf{0}_{p_m \times K_1}, \dots, \mathbf{0}_{p_m \times K_{m-1}}, \boldsymbol{\Gamma}_m, \mathbf{0}_{p_m \times K_{m+1}}, \dots, \mathbf{0}_{p_m \times K_M}] \\ \tilde{\boldsymbol{\eta}}_i &= [\boldsymbol{\eta}_i, \boldsymbol{\phi}_{1i}, \dots, \boldsymbol{\phi}_{Mi}] \quad \tilde{\boldsymbol{\theta}} = [\boldsymbol{\theta}^\top, \mathbf{0}_{K_1}^\top, \dots, \mathbf{0}_{K_M}^\top]^\top,\end{aligned}$$

Crucially, this would leave unchanged quantities in equation (2) as well as the conditional distribution of the response $y_i | \mathbf{x}_i$, due to the blocks of zeros in $\tilde{\boldsymbol{\Lambda}}_m$ and $\tilde{\boldsymbol{\theta}}$. This makes specific factors unidentifiable against shared ones unless the sparsity pattern is known, which is not the case in most applications.

The naive modeling choice in terms of a single set of global factors is made, for instance, in MOFA (Multi-Omics Factor Analysis, Argelaguet et al. 2018). While at first glance the unstructured model might seem to provide a more general formulation, it decreases interpretability by lacking a way to infer block sparsity under an inflated number of shared factors. In contrast, the aforementioned issue of unidentifiability affects alternative contributions in the literature that aim to introduce view-specific latent factors, such as BSFP (Bayesian Simultaneous Factorization and Prediction, Samorodnitsky et al. 2024). BSFP allows the response y_i to load on all $\boldsymbol{\phi}_m$'s as well by having $\tilde{\boldsymbol{\theta}} = [\hat{\boldsymbol{\theta}}^\top, \hat{\boldsymbol{\theta}}_1^\top, \dots, \hat{\boldsymbol{\theta}}_M^\top]^\top$ with non-zero $\hat{\boldsymbol{\theta}}_m$'s, but neglects the aforementioned identifiability issues. Figure 1 further depicts the equivalence between additive local-global factor models and global-only factor models with an appropriate sparsity pattern in the loading matrices.

Identifiability of the local versus global components of the model is of substantial practical importance. There is a parallel literature on multi-study factor models that also have local and global components (Vito

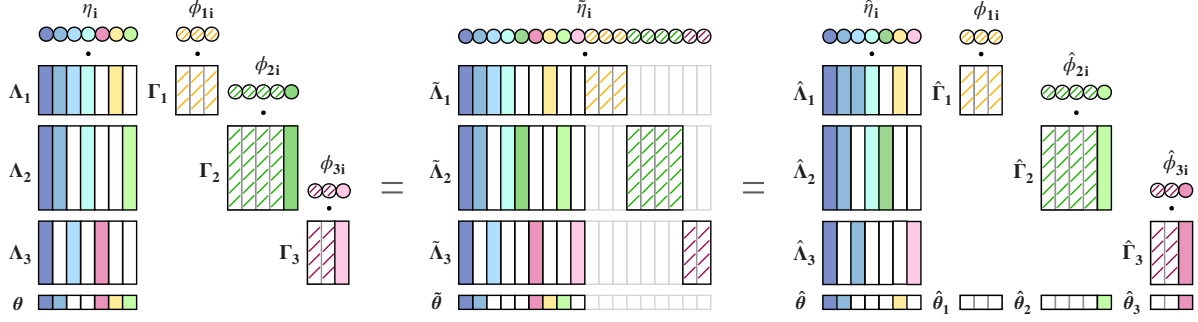


Figure 1: Additive factor models suffer from a specific form of non-identifiability, as formulations with global-local latent factors could be re-expressed as a global-only block-sparse version. The three panels depict the loading matrices of potentially equivalent modeling formulations corresponding to JAFAR, MOFA, and BSFP, respectively. White boxes represent blocks of zero loadings, signaling the inactivity of the corresponding factor in a given data component. Isolating view-specific factors that account for realistic spurious sources of variation (e.g. measurement instrument effects) enhances interpretability and computations. However, a coherent and well-defined formulation requires ensuring identifiability against the shared component.

et al. 2021); in this context, the benefits of imposing identifiability have been clearly shown by Roy et al. (2021) and Chandra, Dunson & Xu (2023) who proposed resolving such an issue via structural modifications of the original modeling formulation. Here we take a different approach, achieving identifiability via a suitable prior structure for the loadings of the shared component in equation (1).

2.1 Prior formulation

To maintain computational tractability in high dimensions, we assume conditionally conjugate priors for most components of the model.

$$\begin{aligned} \eta_i &\stackrel{\text{iid}}{\sim} \mathcal{N}_K(\mathbf{0}_K, \mathbf{I}_K) & \mu_y &\stackrel{\text{iid}}{\sim} \mathcal{N}(0, v_y^2) & \sigma_y^2 &\stackrel{\text{iid}}{\sim} \text{InvGa}(a^{(y)}, b^{(y)}) \\ \phi_{mi} &\stackrel{\text{iid}}{\sim} \mathcal{N}_{K_m}(\mathbf{0}_{K_m}, \mathbf{I}_{K_m}) & \mu_{mj} &\stackrel{\text{iid}}{\sim} \mathcal{N}(0, v_m^2) & \sigma_{mj}^2 &\stackrel{\text{iid}}{\sim} \text{InvGa}(a^{(m)}, b^{(m)}) \end{aligned}$$

We assume independent standard normal priors for all factors, consistently with standard practice. By InvGa and \mathcal{Be} we denote the inverse gamma and the beta distributions, respectively. To impose identifiability, we propose an extension of the CUSP prior of Legramanti et al. (2020). CUSP adaptively removes unnecessary factors from an over-fitted factor model by progressively shrinking the loadings to zero. This is achieved by leveraging stick-breaking representations of Dirichlet processes (Ishwaran & James 2001). We assume independent CUSP priors for the view-specific loadings $\Gamma_m \sim \text{CUSP}(a_m^{(\Gamma)}, b_m^{(\Gamma)}, \tau_{m\infty}^2, \alpha_m^{(\Gamma)})$, with

$$\Gamma_{mjh} \sim \mathcal{N}(0, \tau_{mh}^2) \quad \tau_{mh}^2 \sim \pi_{mh} \text{InvGa}(a_m^{(\Gamma)}, b_m^{(\Gamma)}) + (1 - \pi_{mh}) \delta_{\tau_{m\infty}^2}.$$

Accordingly, the increasing shrinkage behavior is induced by the weight of the spike and slab

$$\pi_{mh} = 1 - \sum_{l=1}^h \omega_{ml} \quad \omega_{mh} = \nu_{mh} \prod_{l=1}^{h-1} (1 - \nu_{ml}) \quad \nu_{mh} \sim \mathcal{Be}(1, \alpha_m^{(\Gamma)}),$$

such that $\mathbb{P}[|\Gamma_{mjh+1}| \leq \varepsilon] > \mathbb{P}[|\Gamma_{mjh}| \leq \varepsilon]$, $\forall \varepsilon > 0$, provided that $b_m^{(\Gamma)}/a_m^{(\Gamma)} > \tau_{m\infty}^2$. The stick-breaking process can be rewritten in terms of discrete latent indicators $\zeta_{mh} \in \mathbb{N}$, where a priori $\mathbb{P}[\zeta_{mh} = l] = \omega_{ml}$ for each $h, l \geq 1$, such that $\pi_{mh} = \mathbb{P}[\zeta_{mh} > h]$. The h^{th} column is defined as active when it is sampled from the slab, namely if $\zeta_{mh} > h$, and inactive otherwise. It is standard practice to truncate the number of factors to conservative upper bounds K_m . This retains sufficient flexibility while allowing for tractable posterior inference via a conditionally conjugate Gibbs sampler. The upper bounds can be tuned as part of the inferential procedure via an adaptive Gibbs sampler. This amounts to dropping the inactive columns of Λ_m while preserving a buffer inactive factor in the rightmost column, provided that suitable diminishing adaptation conditions are satisfied (Roberts & Rosenthal 2007).

2.1.1 Dependent cumulative shrinkage processes (D-CUSP)

We tackle non-identifiability between shared and view-specific factors via a novel joint prior structure for the shared loading matrices $\{\Lambda_m\}_{m=1}^M$ and factor regression coefficients θ . We place zero prior mass on configurations where any shared factor is active in less than two model components. Similar to the spike and slab structure in the original CUSP formulation, we let

$$\begin{aligned}\Lambda_{mjh} &\sim \mathcal{N}(0, \chi_{mh}^2) & \chi_{mh}^2 &\sim \psi_{mh} \text{InvG}a(a_m^{(\Lambda)}, b_m^{(\Lambda)}) + (1 - \psi_{mh}) \delta_{\chi_{m\infty}^2} \\ \theta_h &\sim \mathcal{N}(0, \chi_h^2) & \chi_h^2 &\sim \psi_h \delta_{\chi_o^2} + (1 - \psi_h) \delta_{\chi_\infty^2} & \chi_o^2 &\sim \text{InvG}a(a^{(\theta)}, b^{(\theta)}),\end{aligned}$$

where now we introduce dependence across the views and response via the spike and slab mixture weights ψ_h and $\{\psi_{mh}\}_{m=1}^M$. This can be done by leveraging the representation in terms of latent indicator variables $\{\{\delta_{mh}\}_{h \geq 1}\}_{m=1}^M$ and $\{\delta_h\}_{h \geq 1}$, where $\delta_{mh} \in \mathbb{N}$ and $\delta_h \in \{0, 1\}$. As before, each column of the loading matrices will be sampled from the spike or slab depending on these indicators. Accordingly, it is reasonable to enforce that the h^{th} factor $\eta_{\bullet h}$ is included in the shared variation part of equation (1) if and only if the corresponding loadings are active in at least two components of the model, either 2+ views or 1+ view and the response. Here the notation \bullet in matrices subscripts is used to indicate looping over all indices possible values along a given dimension, whenever the corresponding row- or column-vector has not been previously defined independently.

To maintain increasing shrinkage across the columns of the loadings matrices to adaptively select the correct number of shared factors, we set

$$\begin{aligned}\psi_{mh} &= \mathbb{P}[\{\delta_{mh} > h\} \cap \{\{\delta_h = 1\} \cup \{\bigcup_{m' \neq m} \{\delta_{m'h} > h\}\}\}] \\ &= \mathbb{P}[\delta_{mh} > h] \mathbb{P}[\{\delta_h = 1\} \cup \{\bigcup_{m' \neq m} \{\delta_{m'h} > h\}\}] \\ &= \mathbb{P}[\delta_{mh} > h] \left(1 - \mathbb{P}[\{\delta_h = 0\} \cap \{\bigcap_{m' \neq m} \{\delta_{m'h} \leq h\}\}]\right) \\ &= \mathbb{P}[\delta_{mh} > h] \left(1 - \mathbb{P}[\delta_h = 0] \prod_{m' \neq m} \mathbb{P}[\delta_{m'h} \leq h]\right)\end{aligned}$$

and

$$\psi_h = \mathbb{P}[\{\delta_h = 1\} \cap \{\bigcup_{m'} \{\delta_{m'h} > h\}\}] = \mathbb{P}[\delta_h = 1] \left(1 - \prod_{m'} \mathbb{P}[\delta_{m'h} \leq h]\right),$$

while, analogously to the original CUSP construction, a priori we set

$$\begin{aligned}\mathbb{P}[\delta_{mh} = l] &= \xi_{ml} & \xi_{mh} &= \rho_{mh} \prod_{l=1}^{h-1} (1 - \rho_{ml}) & \rho_{mh} &\sim \mathcal{Be}(1, \alpha_m^{(\Lambda)}) \\ \mathbb{P}[\delta_h = 0] &= \xi & \xi &\sim \mathcal{Be}(a^{(\xi)}, b^{(\xi)}).\end{aligned}$$

We refer to the resulting prior as the dependent CUSPs (D-CUSP) prior. Coherently with the rationale above, the probability of any shared factor $\eta_{\bullet h}$ being inactive reads

$$\begin{aligned}\mathbb{P}[\eta_{\bullet h} \text{ inactive}] &= \mathbb{P}[\mathbb{1}_{(\delta_h=1)} + \sum_m \mathbb{1}_{(\delta_{mh}>h)} \leq 1] \\ &= \mathbb{P}[\mathbb{1}_{(\delta_h=1)} + \sum_m \mathbb{1}_{(\delta_{mh}>h)} = 0] + \mathbb{P}[\mathbb{1}_{(\delta_h=1)} + \sum_m \mathbb{1}_{(\delta_{mh}>h)} = 1] \\ &= \mathbb{P}[\delta_h = 0] \prod_m \mathbb{P}[\delta_{mh} \leq h] + \mathbb{P}[\delta_h = 1] \prod_m \mathbb{P}[\delta_{mh} \leq h] + \mathbb{P}[\delta_h = 0] \mathbb{P}[\sum_m \mathbb{1}_{(\delta_{mh}>h)} = 1] \\ &= \prod_m \mathbb{P}[\delta_{mh} \leq h] + \mathbb{P}[\delta_h = 0] \sum_m \mathbb{P}[\delta_{mh} > h] \prod_{m' \neq m} \mathbb{P}[\delta_{m'h} \leq h],\end{aligned}$$

where $\mathbb{1}_{(C)}$ denotes the indicator function, taking the value 1 if the condition C is satisfied and 0 otherwise. The above quantity can be used to compute the prior expectation for the number of shared factors K_o , which is helpful in eliciting hyperparameters α_m of the stick-breaking process:

$$\begin{aligned}\mathbb{E}[K_o] &= \mathbb{E}\left[\sum_{h=1}^{\infty} (1 - \mathbb{P}[\eta_{\bullet h} \text{ inactive}])\right] \\ &= \sum_{h=1}^{\infty} \left(1 - \prod_{m=1}^M \left(1 - \left(\frac{\alpha_m}{1 + \alpha_m}\right)^h\right) - \frac{a^{(\xi)}}{a^{(\xi)} + b^{(\xi)}} \sum_{m=1}^M \left(\frac{\alpha_m}{1 + \alpha_m}\right)^h \prod_{m' \neq m} \left(1 - \left(\frac{\alpha_{m'}}{1 + \alpha_{m'}}\right)^h\right)\right).\end{aligned}$$

Contrarily to the original CUSP construction, $\mathbb{E}[K_o]$ does not admit a closed-form expression, although it can be trivially computed for any values of the hyperparameters. As before, we consider a truncated version of the D-CUSP construction for practical reasons, by setting a suitable finite upper bound K on the number of shared factors. The hyperparameter K can still be tuned adaptively in the Gibbs sampler, where now we drop the columns of θ and of all $\{\Lambda_m\}_m$ that are either active for only one component of the model or inactive in all of them.

2.1.2 Identifiability of effectively shared factors under D-CUSP

The proposed D-CUSP construction induces the identification of shared and view-specific latent factors in additive factor models for multiview data. The D-CUSP prior puts zero mass on any configuration in which any h^{th} column of the loadings has signals in only one view, while that of all other views and the response are inactive. Such a property is particularly desirable in healthcare applications, such as in Section 4, given the interest in reliable identification of clinically actionable biomarkers. Unstructured priors for the loadings matrix of the shared component, such as BFSP or JAFAR under independent CUSP priors on each view, face practical problems due to their lack of identification restriction. For example, our empirical analyses show that, under independent CUSP priors on the loadings Λ_m , the posterior distribution tends to always saturate at the maximum number of allowed shared factors, even for large upper bounds. This is intuitive given that nominally shared factors have more descriptive power than view-specific ones. Interestingly, our results suggest that the negative consequences of such an issue are not only limited to the mixing of the MCMC chain. Indeed, improper factor allocation is empirically associated with a worse fit to the multiview data, compared to that for the proposed D-CUSP prior.

2.2 Posterior inference via partially collapsed Gibbs sampler

Under the proposed extension of the CUSP construction to the multiview case, the linear-response version of JAFAR still allows for straightforward Gibbs sampling via conjugate full conditionals, detailed in Appendix A. Most of the associated full conditionals take the same forms as those of a regular factor regression model under the CUSP prior. The main difference concerns sampling the latent indicators for the loadings matrix in the shared component of the model. The latter can potentially be sampled from the joint full-conditional $\mathbb{P}[\delta_h = s_h, \{\delta_{mh} = s_{mh}\}_{m=1}^M \mid -]$ for each $h = 1, \dots, K$, where the hyphen “-” is a shorthand to specify the conditioning on all other variables, while $s_h \in \{0, 1\}$ and $s_{mh} \in \{1, \dots, K\}$. This would entail the evaluation of $K \cdot (2 \cdot K^M)$ probabilities for each Gibbs sampler iteration. We instead suggest targeting sequentially $\mathbb{P}[\delta_h = s_h \mid \{\delta_{mh} = s_{mh}\}_{m=1}^M, -]$ and $\mathbb{P}[\delta_{mh} = s_{mh} \mid \delta_h = s_h, \{\delta_{m'h} = s_{m'h}\}_{m' \neq m}, -]$, cutting down the number of required probabilities to $K \cdot (2 + K \cdot M)$. We found the associated efficiency gain and mixing loss trade-off to be greatly beneficial in practical applications.

Although Gibbs sampling is simple to implement, simple one-at-a-time updates can face slow mixing in factor models. We propose two modifications to head off such problems, leading to a partially collapsed Gibbs sampler (Park & van Dyk 2009).

2.2.1 Joint sampling of shared and view-specific loadings

First, for each $m = 1, \dots, M$ and $j = 1, \dots, p_m$, $[\Lambda_{mj\bullet}, \Gamma_{mj\bullet}]$ can be sampled jointly from a $(K + K_m)$ -dimensional normal distribution. Conversely, sampling them from two separate K and K_m -dimensional normals would be detrimental to good mixing because of the interdependence between $\Gamma_{mj\bullet}$ and $\Lambda_{mj\bullet}$. In the case of MOFA, the equivalent step would have cost $\mathcal{O}((K + \sum_{m=1}^M K_m)^3)$.

Conducting similar joint updates for overall response coefficients θ under both the MOFA or BSFP constructions has the $\mathcal{O}((K + \sum_{m=1}^M K_m)^3)$ cost of sampling from a $(K + \sum_{m=1}^M K_m)$ -dimensional normal. The JAFAR structure naturally overcomes this issue, since sampling the coefficients θ requires only dealing with a K -dimensional normal at K^3 cost.

2.2.2 Marginalization of view-specific factors

Secondly, the partially collapsed nature of the proposed Gibbs sampler arises from the update of the latent factors. In fact, for each $i = 1, \dots, n$, a naive Gibbs sampler would either sample them jointly from $\mathbb{P}[\eta_i, \{\phi_{mi}\}_{m=1}^M \mid -]$ at $\mathcal{O}((K + \sum_{m=1}^M K_m)^3)$ -cost (equivalent to MOFA) or sample them sequentially from $\mathbb{P}[\eta_i \mid \{\phi_{mi}\}_{m=1}^M, -]$ and $\mathbb{P}[\phi_{mi} \mid \eta_i, \{\phi_{m'i}\}_{m' \neq m}, -]$, for each $m = 1, \dots, M$. Instead, we sample jointly while improving mixing and computations via blocking and marginalization, exploiting the factorization

$$\mathbb{P}[\eta_i, \{\phi_{mi}\}_{m=1}^M \mid -] = \mathbb{P}[\{\phi_{mi}\}_{m=1}^M \mid \eta_i, -] \mathbb{P}[\eta_i \mid -] = \left(\prod_{m=1}^M \mathbb{P}[\phi_{mi} \mid \eta_i, -] \right) \mathbb{P}[\eta_i \mid -].$$

Here $\mathbb{P}[\boldsymbol{\eta}_i | -]$ denotes the full conditional of the shared factors in a collapsed version of the model, where all view-specific factors have been marginalized out. The structure of JAFAR facilitates the marginalization of the ϕ_{mi} 's. In contrast, the interdependence created by the response component in BSFP leads to a $\mathcal{O}((\sum_{m=1}^M K_m)^3)$ cost for the update of $\mathbb{P}[\boldsymbol{\eta}_i | -]$, as opposed to the $\mathcal{O}(\sum_{m=1}^M K_m^3)$ for JAFAR. Furthermore, the term $\mathbb{P}[\{\phi_{mi}\}_{m=1}^M | \boldsymbol{\eta}_i, -]$ does not factorize over m in BSFP, still due to the response part, leading to a second $\mathcal{O}((\sum_{m=1}^M K_m)^3)$ -cost update.

The same rationale applies to the extensions of JAFAR presented in Appendix B, addressing flexible response modeling via interaction terms and splines. In such cases, the conditional conjugacy of the specific factors is preserved, while the shared factors can be sampled via a Metropolis-within-Gibbs step targeting the associated full conditional in the collapsed model.

2.2.3 Missing Data

In many applications, such as multi-omics data, a significant proportion of features may have missing measurements. Missingness can occur in blocks, where certain modalities are measured only for specific subgroups of subjects. Factor model formulations naturally handle missing data, because the joint model defined for all the covariates and the response can be used to obtain likelihood contributions for data vectors with missing elements under the missing at random assumption without needing to impute missing values. The specific structure of JAFAR is particularly advantageous in this context in leading to easy calculations of the relevant likelihoods and posterior sampling steps under arbitrary missing data patterns. We can also easily impute missing observations from their full conditional posterior distributions within a Gibbs sampler. However, we advise against using the resulting completed data in updating other model unknowns, as it leads to worse mixing than conditioning on the observed data directly in the posterior sampling steps.

2.3 Postprocessing and Multiview MatchAlign

Despite having addressed the identifiability of shared versus view-specific factors, the loading matrices still suffer from rotational ambiguity, label switching and sign switching. These are notorious issues of latent factor models, particularly within the Bayesian paradigm (Poworoznek et al. 2021). Indeed, it is easy to verify that the induced joint covariance decomposition is not unique. Consider semi-orthogonal matrices \mathbf{R} and $\{\mathbf{P}_m\}_m$, respectively of dimensions $K \times K$ and $\{K_m \times K_m\}_m$. Then, the transformed set of loadings $\ddot{\mathbf{\Lambda}}_m = \mathbf{\Lambda}_m \mathbf{R}$ and $\ddot{\mathbf{\Gamma}}_m = \mathbf{\Gamma}_m \mathbf{P}_m$ clearly satisfy $\ddot{\mathbf{\Lambda}}_m \ddot{\mathbf{\Lambda}}_{m'}^\top = \mathbf{\Lambda}_m \mathbf{\Lambda}_{m'}^\top$ and $\ddot{\mathbf{\Gamma}}_m \ddot{\mathbf{\Gamma}}_{m'}^\top = \mathbf{\Gamma}_m \mathbf{\Gamma}_{m'}^\top$ for every $m, m' = 1, \dots, M$, which leaves $\text{cov}(\mathbf{x}_m)$ and $\text{cov}(\mathbf{x}_m, \mathbf{x}_{m'})$ unaffected. Concurrently, adequately transforming $\boldsymbol{\theta}$ and $\boldsymbol{\eta}_i$ to $\ddot{\boldsymbol{\theta}} = \boldsymbol{\theta} \mathbf{R}$ and $\ddot{\boldsymbol{\eta}}_i = \mathbf{R}^\top \boldsymbol{\eta}_i$ preserves predictions of the response y_i . Such non-identifiability is particularly problematic when there is interest in inferring the latent variables and corresponding factor loadings. Several contributions in the literature have addressed this problem. MatchAlign (Poworoznek et al. 2021) provides an efficient post-processing algorithm, which first applies Varimax (Kaiser 1958) to every loadings sample to orthogonalize, fixing optimal rotations according to a suitable objective function. While this solves rotational ambiguity, the loadings samples still suffer from non-identifiability with respect to column labels and sign switching. Accordingly, the authors propose to address both issues in a second step, by matching and aligning each posterior sample to a reference via a greedy maximization procedure.

2.3.1 Multiview Varimax

To address rotational ambiguity, label switching and sign switching, MatchAlign could be applied to MCMC samples of the stacked loadings matrices $\mathbf{\Lambda} = [\mathbf{\Lambda}_1^\top, \dots, \mathbf{\Lambda}_M^\top, \boldsymbol{\theta}_0^\top]^\top$ and view-specific $\mathbf{\Gamma}_m = [\mathbf{\Gamma}_m, \boldsymbol{\theta}_m^\top]^\top$, for each $m = 1, \dots, M$. However, a more elaborate approach can be beneficial in multiview scenarios. A side-benefit of Varimax is inducing row-wise sparsity in the loadings matrices, which in turn allows for clearer interpretability of the role of different latent sources of variability. This is because, given any $p \times K$ loading matrix $\mathbf{\Lambda}$, the Varimax procedure solves the optimization problem $\mathbf{R}_o = \arg\max_{\mathbf{R} \in \mathbb{R}^{K \times K}: \mathbf{R}\mathbf{R}^\top = \mathbf{I}_K} V(\mathbf{\Lambda}, \mathbf{R})$, where

$$V(\mathbf{\Lambda}, \mathbf{R}) = \frac{1}{p} \sum_{h=1}^K \sum_{j=1}^p (\mathbf{\Lambda} \mathbf{R})_{jh}^4 - \sum_{h=1}^K \left(\frac{1}{p} \sum_{j=1}^p (\mathbf{\Lambda} \mathbf{R})_{jh}^2 \right)^2.$$

Accordingly, \mathbf{R}_o is the optimal rotation matrix maximizing the sum of the variances of the squared loadings. Intuitively, this is achieved under two conditions. First, any given \mathbf{x}_j has large loading Λ_{jh^*} on a single factor h^* , but near-zero loadings Λ_{j-h^*} on the remaining $K - 1$ factors. Secondly, any h^{th} factor is loaded on by only a small subset $\mathcal{J}_h \subset \{1, \dots, p\}$ of variables, having high loadings $\Lambda_{\mathcal{J}_h h}$ on such a factor, while the loadings $\Lambda_{-\mathcal{J}_h h}$ associated with the remaining $\{1, \dots, p\} \setminus \mathcal{J}_h$ variables are close to zero. However, when applied to the stacked shared loadings of JAFAR, such a sparsity-inducing mechanism can disrupt the very structure for which the models were designed. This is because a naive application of `Varimax` to the stacked loadings is likely to favor representations in which each factor is effectively loaded only by a subset of variables \mathbf{x}_m from a single view, in an effort to minimize the cardinality of $|\mathcal{J}_h|$ for every $h = 1, \dots, K$. This destroys the interpretation of shared factors as latent sources of variations affecting multiple components of the data.

Hence, we suggest instead solving $\mathbf{R}_* = \operatorname{argmax}_{\mathbf{R} \in \mathbb{R}^{K \times K} : \mathbf{R}\mathbf{R}^\top = \mathbf{I}_K} \sum_{m=1}^M V(\Lambda_m, \mathbf{R})$, with

$$\sum_{m=1}^M V(\Lambda_m, \mathbf{R}) = \sum_{m=1}^M \left(\frac{1}{p_m} \sum_{h=1}^K \sum_{j=1}^{p_m} (\Lambda_m \mathbf{R})_{jh}^4 - \sum_{h=1}^K \left(\frac{1}{p_m} \sum_{j=1}^{p_m} (\Lambda_m \mathbf{R})_{jh}^2 \right)^2 \right) \quad (3)$$

representing the sum of the within-view squared loadings sum of variances, after applying any rotation \mathbf{R} . Accordingly, this is expected to enforce sparsity within each view, but not across views. Optimization of the modified target entails trivial modification of the original routine.

3 Simulation Studies

To assess the performance of JAFAR under the D-CUSP prior, we first conducted simulation experiments. These experiments involved generating data from a factor model with the additive structure outlined in equation (1). We considered 10 independent replicated datasets, each with $M = 3$ views of dimensions $p_m = \{100, 200, 300\}$, for increasing sample sizes $n \in \{50, 100, 200, 500\}$ and fixed test set size $n_{test} = 100$. Such values were chosen to preserve a $p \gtrsim n$ setup and to create challenging test cases. The assumed number of shared factors was set to $K^{(true)} = 15$, with the responses loading on 9 of them, while the view-specific ones were $\{K_m^{(true)}\}_{m=1}^M = \{8, 9, 10\}$. To create realistic simulations that mimic real-world multiview data, we propose a novel scheme for generating loading matrices. These matrices induce sensible block-structured correlations, as described in Appendix C. To test the identification of prediction-relevant features, only half of the features from each view were allowed to have non-zero loadings on response-related factors.

Given the generated the loading matrices Λ_m and Γ_m , we sample the target signal-to-noise ratios $\{\text{snr}_{mj}\}_{j=1}^{p_m}$ from an inverse gamma distribution $\text{InvGa}(10, 30)$, and set accordingly each idiosyncratic variances to $\sigma_{mj}^2 (\Lambda_m \Lambda_m^\top + \Gamma_m \Gamma_m^\top)_{jj} / \text{snr}_{mj}$, $\forall j = 1, \dots, p_m$. Analogous to the loading matrices generation from Appendix C, the absolute value of the active response coefficients θ_h was sampled from a beta distribution $\text{Be}(5, 3)$, and their signs were randomly assigned with equal probability. The response variance σ_y^2 was adjusted such that the signal-to-noise ratio $\theta^\top \theta / \sigma_y^2$ equals 1. Both the multiview features and the response were standardized before the analysis to have mean zero and unit variance.

We compare JAFAR to BSFP, whereas their paper provided a recent comparison to alternative latent factorization approaches showing state-of-the-art performance (Samorodnitsky et al. 2024). We also consider two other non-factor models alternatives: Cooperative Learning (`CoopLearn`) and IntegratedLearner (`IntegLearn`). `CoopLearn` complements usual squared-error loss-based predictions with an agreement penalty, which encourages predictions coming from separate data views to match with one another. We set the associated agreement parameter to $\rho_{CL} = 0.5$. `IntegLearn` combines the predictions of Bayesian additive regression trees (BART) fit separately to each view, where we use the default late fusion scheme to integrate the individual models.

We run BSFP under the default setup and hyperparameters from the official implementation. This entails setting $\sigma_{mj}^2 = 1$ after rescaling the data to have unit error variance (rather than unit overall variance) using the median absolute deviation estimator (Gavish & Donoho 2017). The default prior on σ_y^2 corresponds to $a^{(y)} = b^{(y)} = 0.01$. Contrary to Section 2.1, the priors on each entry of both shared factors η_{ih} and loadings

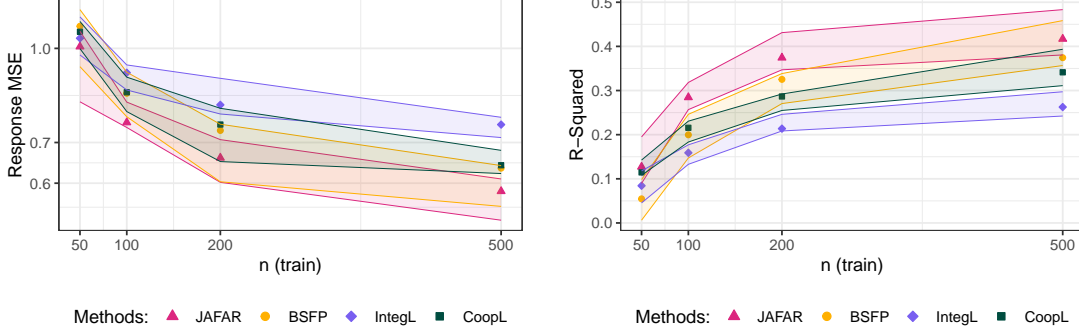


Figure 2: Mean squared error (in logarithmic scale) of the predicted responses in the test sets of simulated data. The x-axis reports increasing size of the train set. The interior points and band edges correspond to the quartiles over 10 independent replicates for fixed dimensions.

Λ_{mjh} are independent normal distributions with zero mean and variance $r_o^2 = (\sqrt{n} + \sqrt{\sum_m p_m})^{-1}$. Similarly, the priors on each entry of both view-specific factors ϕ_{mih} and loadings Γ_{mjh} are independent normal distributions with zero mean and variances $r_m^2 = (\sqrt{n} + \sqrt{p_m})^{-1}$. They use a UNIFAC initialization, which retains singular values greater than r_o^2 and r_m^2 in the joint and individual components, respectively. The authors further set $\nu_y^2 = 1000$ and $\chi_h^2 = 1$, while the absence of the intercept in the predictors corresponds to the limit $\nu_m^2 \rightarrow 0$.

For JAFAR, we initialized the number of factors to $K^{\text{MAX}} = 40$ and $\{K_m^{\text{MAX}}\}_{m=1}^M = \{30, 30, 30\}$. Similarly to the original CUSP construction, such values must be chosen to provide conservative upper bounds to the true number of latent factors. The hyperparameters of the D-CUSP prior were set to the values in Equation 4.

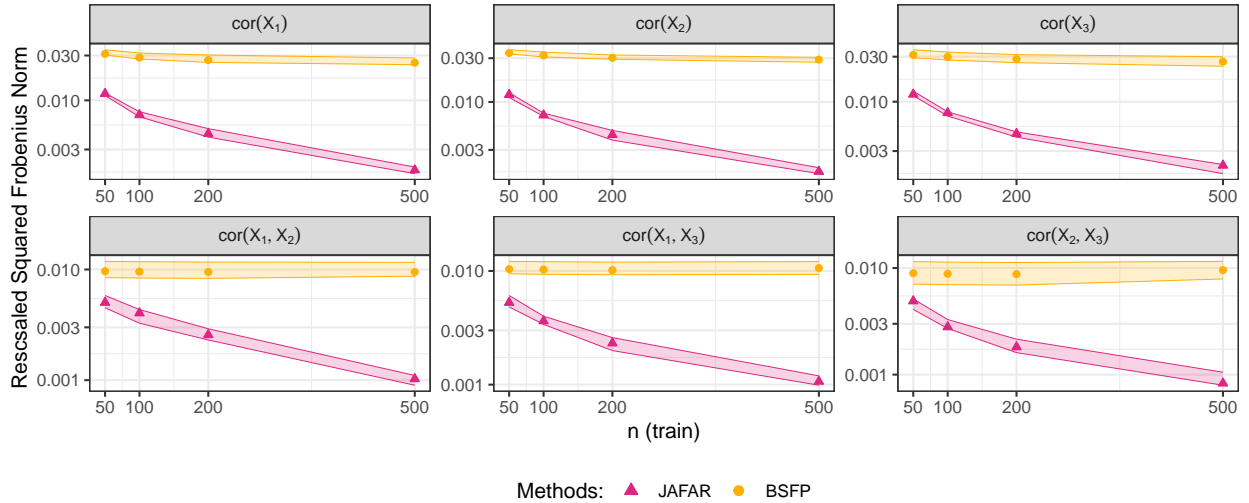


Figure 3: Frobenius norms of the differences between the true and inferred correlations for the simulated data. The two rows report the inter and intra-view correlations, respectively. All norms have been rescaled by the dimensions of the corresponding matrices. The interior points and band edges correspond to the quartiles over 10 independent replicates for fixed dimensions.

Data distributions	$a^{(y)} = a^{(m)} = 3$	$b^{(y)} = b^{(m)} = 1$	$v_y^2 = v_m^2 = 4$	(4)
Predictors Spike & slab variances	$a_m^{(\tau)} = a_m^{(\Lambda)} = 0.5$	$b_m^{(\tau)} = b_m^{(\Lambda)} = 0.1$	$\tau_{m\infty}^2 = \chi_{m\infty}^2 = 0.005$	
Response Spike & slab variances	$a^{(\theta)} = 2$	$b^{(\theta)} = 2$	$\chi_\infty^2 = 0.05$	
Spike & slab weights	$a^{(\xi)} = 3$	$b^{(\xi)} = 2$	$\alpha_m^{(\tau)} = \alpha_m^{(\Lambda)} = 5$	

The prior parameters for σ_y^2 and σ_m^2 are meant to favor small values for σ_y^2 , encouraging the model to explain a substantial part of the variability through the signal components rather than via noise. The hyperparameters of the spike-and-slab on the response loadings are the same as the original contribution by Legramanti et al. (2020), while those of the predictors are essentially a shrunk version thereof. Indeed, our empirical results suggest that, high-dimensional scenarios, better performances are achieved by inducing smaller values of the loadings both for active and inactive columns, while still allowing for a clear separation of the two components. Notably, the proposed set of parameters leads to superior feature reconstructions for CUSP itself when applied to each separate view in the absence of the response. The choice of $a^{(\xi)}$ and $b^{(\xi)}$ reflects a slight prior preference for the active entries θ_h in the response loadings, rather than inactive, without increasing shrinkage on h . We refer to Legramanti et al. (2020) for further insights on the role of the hyperparameters. Our results reduced sensitivity to the choice of $\alpha_m^{(\Lambda)}$ and $\alpha_m^{(\tau)}$.

We run the Gibbs samplers of JAFAR for a total of $T_{\text{MCMC}} = 10000$ iterations, with a burn-in of $T_{\text{BURN-IN}} = 6000$ steps and thinning every $T_{\text{thin}} = 10$ samples for memory efficiency. As BSFP comes with significantly higher computing times, we set $T_{\text{MCMC}} = 5000$ and $T_{\text{BURN-IN}} = 2500$, while keeping $T_{\text{thin}} = 10$. The average computation times for $n = 500$ under the above settings were 10 and 45 minutes for JAFAR and BSFP, respectively, on a 13-inch MacBook Pro (2018) with a 2.7 GHz quad-core Intel Core i7 processor and 16Gb RAM (macOS 14.6.1). This difference is due to a combination of the computational improvements presented in Section 2 and vectorization of the code. For reference, CoopLearn and IntegLearn run in less than 3 seconds and roughly 1.5 minutes on the same machine.

In this setting, JAFAR achieves competitive or superior predictive accuracy than all other methods, as shown in Figure 2. Crucially, this is associated with accurate reconstruction of the dependence structure underlying the data. In Figure 3, we analyzed accuracy in capturing the dependence structure in the multiview features. We focus on the Frobenius norm of the difference between the true and inferred correlation matrices within and between views, associated with equation (2). JAFAR achieves good reconstruction errors, while BSFP suffers from severe overshrinking. Appendix D provides further insight into the corresponding performances in some exemplar replicates.

Notice that, in all factors model formulations, out-of-sample predictions of $\mathbb{E}[y_i \mid \{\mathbf{X}_{mi}\}_{m=1}^M, -]$ can be easily constructed via Monte Carlo averages $\frac{1}{T_{\text{EFF}}} \sum_{t=1}^{T_{\text{EFF}}} \mathbb{E}[y_i \mid \boldsymbol{\eta}_i^{(t)} -]$ exploiting samples from $\boldsymbol{\eta}_i^{(t)} \sim p(\boldsymbol{\eta}_i \mid \{\mathbf{X}_{mi}\}_{m=1}^M, -)$, where T_{EFF} is the number of MCMC samples after burn-in and thinning. To ensure coherence in this analysis, it was necessary to modify the function `bsfp.predict` from the main BSFP GitHub repository. Indeed, the default implementation considers only samples from $p(\boldsymbol{\eta}_i \mid y_i, \{\mathbf{X}_{mi}\}_{m=1}^M, -)$ and $p(\boldsymbol{\phi}_{mi} \mid y_i, \mathbf{X}_{mi}, -)$, whereas conditioning on the response is ill-posed in our settings. The updated code is available in the JAFAR GitHub repository.

4 Labor onset prediction from immunome, metabolome & proteome

To further showcase the performance of the proposed methodology on real data, we focus on predicting time-to-labor onset from immunome, metabolome, and proteome data for a cohort of women who went into labor spontaneously. The dataset, available in the GitHub repository associated with Mallick et al. (2024), considers repeated measurements during the last 100 days of pregnancy for 63 women. Similar to Ding et al. (2022), we obtained a cross-sectional sub-dataset by considering only the first measurement for each woman and we treat time-to-labor onset as a continuous outcome. We dropped 10 subjects for which only immunome data were available and split the remaining 53 observations into training and test sets of $n_{\text{train}} = 40$ and $n_{\text{test}} = 13$ subjects, respectively. The dataset falls into a large- p -small- n scenario, as

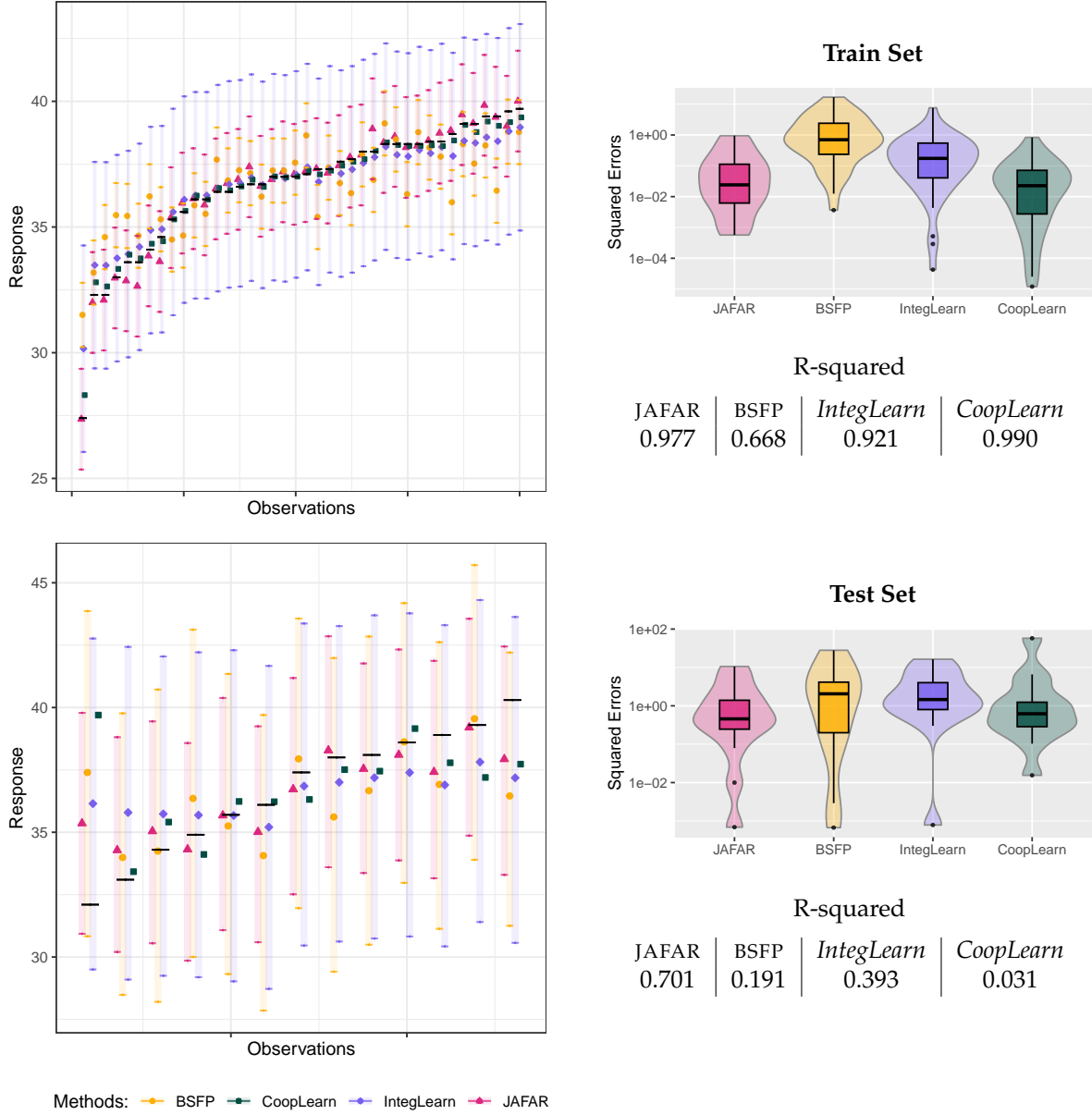


Figure 4: Time-to-labor (days) prediction accuracy for the different methods considered. In the plots to the left, the dots and the vertical bars represent the expected values and the 90% credible intervals for the predicted responses, respectively. The black horizontal ticks correspond to the true values of the response for each observation. Both *CoopLearn* and *IntegLearn* achieve good predictive performances in the train set, but do not perform as well on out-of-sample observations. *BSFP* performs worse both in terms of expected values and predictive intervals, which are almost as wide as the effective range of the response. *JAFAR* achieves remarkable generalization error on the test.

the $M = 3$ layers of blood measurements provide information on $p_1 = 1141$ single-cell immune features, $p_2 = 3529$ metabolites, and $p_3 = 1317$ proteins.

As before, we compare *JAFAR* to *BSFP*, Cooperative Learning and the IntegratedLearner, with the same hyperparameters from the previous section. Prior to analysis, we standardized the data and log-transformed the metabolomics and proteomics features. Despite these preprocessing steps, all omics layers exhibited

considerable deviation from Gaussianity, with over 30% of features in each view yielding univariate Shapiro test statistics below 0.95. To address this challenge, we target copula factor model variants (Hoff 2007, Murray et al. 2013) for both JAFAR and BSFP, as detailed in Appendix B. Given the continuous nature of the omics data and the absence of missing entries, the incorporation of the copula layer boils down to a deterministic preprocessing procedure, involving feature-wise transformations that leverage estimates of the associated empirical cumulative distribution functions.

We initialized the number of factors in JAFAR to $K^{\text{MAX}} = 60$ and $\{K_m^{\text{MAX}}\}_{m=1}^M = \{50, 50, 50\}$ and run the Gibbs sampler for a total of $T_{\text{MCMC}} = 20000$ iterations, with a burn-in of $T_{\text{BURN-IN}} = 15000$ steps and $T_{\text{thin}} = 10$. For BSFP we set $T_{\text{MCMC}} = 10000$ iterations, with a burn-in of $T_{\text{BURN-IN}} = 5000$. On the same machine used for the simulation studies, the runtimes of JAFAR and BSFP were roughly 3.5 and 5 hours, respectively. Although smaller than in the simulations, such relative improvement is even more significant because BSFP considers significantly fewer latent factors than JAFAR, as detailed below.

The relative accuracy in predicting the response values is summarized in Figure 4. JAFAR achieves superior predictive performance over BSFP and IntegLearn and competitive performance with CoopLearning, in both the training and test sets. Despite suffering as well from slight over-coverage, JAFAR improve over BSFP and IntegLearn by reducing the width of out-of-sample predictive intervals. The substandard performance of BSFP can be only partly attributed to the limited number of factors inferred by the UNIFAC initialization, as depicted in Figure 5. JAFAR learns a substantially greater number of factors, particularly in

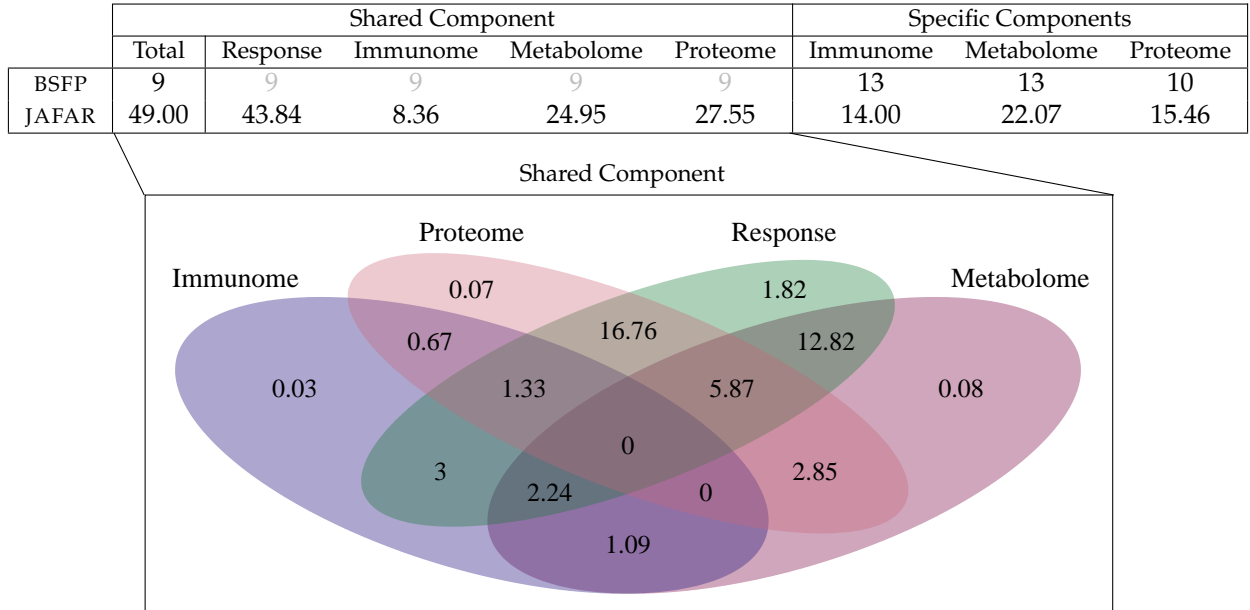


Figure 5: Numbers of inferred active factors by the two additive factor models considered in the time-to-labor application. Here the $M = 3$ omics layers correspond to immunome, metabolome and proteome data respectively. The entries of the table (top) correspond to the fixed ranks inferred via the UNIFAC initialization in BSFP, and to the posterior means of the number of active columns in JAFAR, computed according to the latent indicators in the D-CUSP construction. JAFAR allows to further decompose the activity pattern in the shared factors, which are not required to be active in all data layers. The Venn diagram (bottom) annotates each subregion with the posterior means of the number of shared factors η active in all and only the corresponding overlapping components. The D-CUSP prior is effective in removing view-specific sources of variation from the shared component part of the structure, as near zero factors are active in each omic layer only. A good part of the response variation is explained by factors related to only one view (3.00, 16.76, and 12.82), confirming that integrated analysis captures more signal than individual ones. At the same time, there are response-related factors effectively shared by more than one view (2.24, 1.33, and 5.87), corresponding to effectively shared sources of variation.



Figure 6: Empirical and inferred correlation structures for the three omics layers. The first row reports the empirical correlations on the train set. The second row shows the posterior mean of the correlation matrices associated with the induced covariances $\Lambda_m \Lambda_m^\top + \Gamma_m \Gamma_m^\top + \text{diag}(\sigma_m^2)$ inferred by JAFAR. The third row reports the correlation matrices reconstructed by BSFP via MCMC samples from $p(\mathbf{X}_m \mid \{\mathbf{X}_{m'}\}_{m' \neq m})$. For JAFAR, one could similarly compute correlations from MCMC samples of \mathbf{X}_m , but the induced covariances offer a more elegant approach, highlighting a key advantage of factor models. The induced covariance is less suitable for BSFP due to the unusual scale imposed on the factors by their prior variance, which induces a mismatch between computations made a priori (via marginalization over the latent factors) and a posterior. Either way, BSFP completely fails to accurately reconstruct inter-view correlations, collapsing to diagonal structures. JAFAR, instead, captures the main features of the dependence structure, albeit suffering from mild underestimation, which is not uncommon in extremely high-dimensional scenarios with few observations.

the shared component of the model. The response load on most of the shared axes of variation learned by JAFAR, with all omics bearing predictive power. This intuition is further supported by the induced regression coefficients, reported in Appendix E.

Similar to the simulation studies, JAFAR’s superior performances carry over to the reconstructed dependence structures in the predictors. In Figure 6, we report the empirical and inferred within-view correlation matrices, crucial to ensure meaningful interpretability of the latent sources of variation. The observed slight underestimation of the correlation structure is not uncommon in extremely high-dimensional scenarios. The correlation matrices inferred by BSFP suffer from extreme overshrinking, essentially collapsing to

diagonal structures. In Appendix E we also report the posterior mean of the shared loading matrices after postprocessing using the extended version of `MatchAlign` via `Multiview Varimax`.

5 Discussion

We have developed a novel additive factor regression approach, termed JAFAR, for inferring latent sources of variability underlying dependence in multiview features. JAFAR isolates shared- and view-specific factors, thereby facilitating inference, prediction, and feature selection. To ensure the identifiability of shared sources of variation, we introduce a novel extension of the CUSP prior (Legramanti et al. 2020) and provide an enhanced partially collapsed Gibbs sampler for posterior inference. Additionally, we extend the `Varimax` procedure (Kaiser 1958) to multiview settings, preserving the composite structure of the model to resolve rotational ambiguity.

JAFAR’s performance is compared to state-of-the-art competitors using multiview simulated data and in an application focusing on predicting time-to-labor onset from multiview features derived from immunomes, metabolomes, and proteomes. The carefully designed structure of JAFAR enables accurate learning and inference of response-related latent factors, as well as the inter- and intra-view correlation structures. In the Appendix, we discuss more flexible response modeling through interactions among latent factors (Ferrari & Dunson 2021) and splines, while considering extensions akin to generalized linear models. The benefit of the proposed D-CUSP prior extends to unsupervised scenarios, particularly when the focus is solely on disentangling the sources of variability within integrated multimodal data. To the best of our knowledge, this results in the first fully Bayesian analog of JIVE (Lock et al. 2013). Lastly, analogous constructions can be readily developed using the structured increasing shrinkage prior proposed by Schiavon et al. (2022), allowing for the inclusion of prior annotation data on features.

Acknowledgements

This project has received funding from the European Research Council (ERC) under the European Union’s Horizon 2020 research and innovation program (grant agreement No 856506), and United States National Institutes of Health (R01ES035625, 5R01ES027498-05, 5R01AI167850-03), and was supported in part by Merck & Co., Inc., through its support for the Merck Biostatistics and Research Decision Sciences (BARDS) Academic Collaboration.

References

- Albert, J. & Chib, S. (1993), ‘Bayesian analysis of binary and polychotomous response data’, *Journal of the American Statistical Association* **88**(422), 669–679.
- Argelaguet, R., Velten, B., Arnol, D., Dietrich, S., Zenz, T., Marioni, J. C., Buettner, F., Huber, W. & Stegle, O. (2018), ‘Multi-omics factor analysis — A framework for unsupervised integration of multi-omics data sets’, *Molecular Systems Biology* **14**(6), e8124.
- Carvalho, C. M., Chang, J., Lucas, J. E., Nevins, J. R., Wang, Q. & West, M. (2008), ‘High-dimensional sparse factor modeling: Applications in gene expression genomics’, *Journal of the American Statistical Association* **103**(484), 1438–1456.
- Chandra, N. K., Canale, A. & Dunson, D. B. (2023), ‘Escaping the curse of dimensionality in bayesian model-based clustering’, *Journal of Machine Learning Research* **24**(144), 1–42.
- Chandra, N. K., Dunson, D. B. & Xu, J. (2023), ‘Inferring covariance structure from multiple data sources via subspace factor analysis’, *arXiv preprint arXiv:2305.04113*.
- Ding, D. Y., Li, S., Narasimhan, B. & Tibshirani, R. (2022), ‘Cooperative learning for multiview analysis’, *Proceedings of the National Academy of Sciences* **119**(38), e2202113119.
- Feldman, J. & Kowal, D. R. (2024), ‘Nonparametric copula models for multivariate, mixed, and missing data’, *Journal of Machine Learning Research* **25**(164).

- Ferrari, F. & Dunson, D. B. (2021), 'Bayesian factor analysis for inference on interactions', *Journal of the American Statistical Association* **116**(535), 1521–1532.
- Gavish, M. & Donoho, D. L. (2017), 'Optimal shrinkage of singular values', *IEEE Transactions on Information Theory* **63**(4), 2137–2152.
- Hoff, P. D. (2007), 'Extending the rank likelihood for semiparametric copula estimation', *The Annals of Applied Statistics* **1**(1), 265–283.
- Ishwaran, H. & James, L. F. (2001), 'Gibbs sampling methods for stick-breaking priors', *Journal of the American statistical Association* **96**(453), 161–173.
- Kaiser, H. F. (1958), 'The varimax criterion for analytic rotation in factor analysis', *Psychometrika* **23**(3), 187–200.
- Klaassen, C. A., Wellner, J. A. et al. (1997), 'Efficient estimation in the bivariate normal copula model: normal margins are least favourable', *Bernoulli* **3**(1), 55–77.
- Lee, S. I. & Yoo, S. J. (2020), 'Multimodal deep learning for finance: Integrating and forecasting international stock markets', *The Journal of Supercomputing* **76**, 8294–8312.
- Legramanti, S., Durante, D. & Dunson, D. B. (2020), 'Bayesian cumulative shrinkage for infinite factorizations', *Biometrika* **107**(3), 745–752.
- Li, G. & Jung, S. (2017), 'Incorporating covariates into integrated factor analysis of multi-view data', *Biometrics* **73**(4), 1433–1442.
- Li, Q. & Li, L. (2022), 'Integrative factor regression and its inference for multimodal data analysis', *Journal of the American Statistical Association* **117**(540), 2207–2221.
- Li, R., Ma, F. & Gao, J. (2021), Integrating multimodal electronic health records for diagnosis prediction, in 'AMIA Annual Symposium Proceedings', Vol. 2021, American Medical Informatics Association, p. 726.
- Lock, E. F., Hoadley, K. A., Marron, J. S. & Nobel, A. B. (2013), 'Joint and individual variation explained (JIVE) for integrated analysis of multiple data types', *The Annals of Applied Statistics* **7**(1), 523 – 542.
- Mallick, H., Porwal, A., Saha, S., Basak, P., Svetnik, V. & Paul, E. (2024), 'An integrated Bayesian framework for multi-omics prediction and classification', *Statistics in Medicine* **43**(5), 983–1002.
- McNaboe, R., Beardslee, L., Kong, Y., Smith, B. N., Chen, I.-P., Posada-Quintero, H. F. & Chon, K. H. (2022), 'Design and validation of a multimodal wearable device for simultaneous collection of electrocardiogram, electromyogram, and electrodermal activity', *Sensors* **22**(22), 8851.
- Moran, K. R., Dunson, D. B., Wheeler, M. W. & Herring, A. H. (2021), 'Bayesian joint modeling of chemical structure and dose response curves', *The Annals of Applied Statistics* **15**(3), 1405 – 1430.
- Murray, J. S., Dunson, D. B., Carin, L. & Lucas, J. E. (2013), 'Bayesian gaussian copula factor models for mixed data', *Journal of the American Statistical Association* **108**(502), 656–665.
- Palzer, E. F., Wendt, C. H., Bowler, R. P., Hersh, C. P., Safo, S. E. & Lock, E. F. (2022), 'sjive: Supervised joint and individual variation explained', *Computational Statistics & Data Analysis* **175**, 107547.
- Park, T. & van Dyk, D. A. (2009), 'Partially collapsed gibbs samplers: Illustrations and applications', *Journal of Computational and Graphical Statistics* **18**(2), 283–305.
- Poworoznek, E., Ferrari, F. & Dunson, D. B. (2021), 'Efficiently resolving rotational ambiguity in bayesian matrix sampling with matching', *arXiv preprint arXiv:2107.13783*.
- Roberts, G. O. & Rosenthal, J. S. (2007), 'Coupling and ergodicity of adaptive markov chain monte carlo algorithms', *Journal of applied probability* **44**(2), 458–475.
- Roy, A., Lavine, I., Herring, A. H. & Dunson, D. B. (2021), 'Perturbed factor analysis: Accounting for group differences in exposure profiles', *The Annals of Applied Statistics* **15**(3), 1386 – 1404.
- Samorodnitsky, S., Wendt, C. H. & Lock, E. F. (2024), 'Bayesian simultaneous factorization and prediction using multi-omic data', *Computational Statistics & Data Analysis* **198**(1), In Press.
- Schiavon, L., Canale, A. & Dunson, D. B. (2022), 'Generalized infinite factorization models', *Biometrika* **109**(3), 817–835.

- Sklar, A. (1959), ‘Fonctions de repartition an dimensions et leurs marges’, *Publications de l’Institut de statistique de l’Université de Paris* **8**, 229–231.
- Stelzer, I. A., Ghaemi, M. S., Han, X., Ando, K., Hédou, J. J., Feyaerts, D., Peterson, L. S., Rumer, K. K., Tsai, E. S., Ganio, E. A., Gaudillière, D. K., Tsai, A. S., Choisy, B., Gaigne, L. P., Verdonk, F., Jacobsen, D., Gavasso, S., Traber, G. M., Ellenberger, M., Stanley, N., Becker, M., Culos, A., Fallahzadeh, R., Wong, R. J., Darmstadt, G. L., Druzin, M. L., Winn, V. D., Gibbs, R. S., Ling, X. B., Sylvester, K., Carvalho, B., Snyder, M. P., Shaw, G. M., Stevenson, D. K., Contrepolis, K., Angst, M. S., Aghaeepour, N. & Gaudillière, B. (2021), ‘Integrated trajectories of the maternal metabolome, proteome, and immunome predict labor onset’, *Science Translational Medicine* **13**(592), eabd9898.
- Vito, R. D., Bellio, R., Trippa, L. & Parmigiani, G. (2021), ‘Bayesian multistudy factor analysis for high-throughput biological data’, *The Annals of Applied Statistics* **15**(4), 1723 – 1741.

Appendix A Gibbs Sampler for JAFAR under D-CUSP

In the current Section, we report the details of the implementation of the partially collapsed Gibbs sampler for the linear version of JAFAR, under the proposed D-CUSP prior for the shared loadings matrix $\mathbf{\Lambda}_m$ and response coefficients $\boldsymbol{\theta}$. As before, let us define $\mathbf{Z}_m = [\mathbf{z}_{m1}^\top, \dots, \mathbf{z}_{mn}^\top]^\top \in \mathbb{R}^{n \times p_m}$ for every $m = 1, \dots, M$. We presented the algorithm in terms of the transformed features $\mathbf{z}_{mij} = \Phi^{-1}(\hat{\mathbf{F}}_{mj}(\mathbf{x}_{mij}))$ within the Gaussian copula factor model formulation. Nonetheless, the same structure holds in the absence of the copula layer, by simply replacing \mathbf{z}_{mij} with \mathbf{x}_{mij} .

Algorithm A1: One cycle of the partially collapsed Gibbs sampler for JAFAR with the D-CUSP prior on the shared loadings

1. sample $[\mu_y, \boldsymbol{\theta}]$ from $\mathcal{N}_{1+K}(\mathbf{V}_\theta \mathbf{u}_\theta, \mathbf{V}_\theta)$, where

$$\begin{cases} \mathbf{V}_\theta = (\text{diag}([v_y^{-2}, \{\chi_h^{-2}\}_{h=1}^K]) + \sigma_y^{-2}[\mathbf{1}_n, \boldsymbol{\eta}]^\top [\mathbf{1}_n, \boldsymbol{\eta}])^{-1} \\ \mathbf{u}_\theta = \sigma_y^{-2}[\mathbf{1}_n, \boldsymbol{\eta}]^\top \mathbf{y} \end{cases}$$
2. for $m = 1, \dots, M$:
 - for $j = 1, \dots, p_m$:
 - sample $[\boldsymbol{\mu}_{mj}, \mathbf{\Lambda}_{mj\bullet}, \boldsymbol{\Gamma}_{mj\bullet}]$ from $\mathcal{N}_{1+K+K_m}(\mathbf{V}_{mj} \mathbf{u}_{mj}, \mathbf{V}_{mj})$, where

$$\begin{cases} \mathbf{V}_{mj} = (\text{diag}([v_m^{-2}, \{\chi_{mh}^{-2}\}_{h=1}^K, \{\tau_{mh}^{-2}\}_{h=1}^{K_m}]) + \sigma_{mj}^{-2}[\mathbf{1}_n, \boldsymbol{\eta}, \boldsymbol{\phi}_m]^\top [\mathbf{1}_n, \boldsymbol{\eta}, \boldsymbol{\phi}_m])^{-1} \\ \mathbf{u}_{mj} = \sigma_{mj}^{-2}[\mathbf{1}_n, \boldsymbol{\eta}, \boldsymbol{\phi}_m]^\top \mathbf{Z}_{m\bullet j} \end{cases}$$
3. sample σ_y^2 from $\mathcal{InvGa}(a^{(y)} + 0.5n, b^{(y)} + 0.5 \text{sum}((\mathbf{y} - \mathbf{1}_n \mu_y - \boldsymbol{\eta} \boldsymbol{\theta})^2))$
 - for $m = 1, \dots, M$:
 - for $j = 1, \dots, p_m$:
 - sample σ_{mj}^2 from $\mathcal{InvGa}(a^{(m)} + 0.5n, b^{(m)} + 0.5d_{mj})$, where

$$d_{mj} = \text{sum}((\mathbf{Z}_{m\bullet j} - \mathbf{1}_n \boldsymbol{\mu}_{mj} - \boldsymbol{\eta} \mathbf{\Lambda}_{mj\bullet} - \boldsymbol{\phi}_m \boldsymbol{\Gamma}_{mj\bullet})^2)$$
4. for $i = 1, \dots, n$:
 - sample $\boldsymbol{\eta}_i$ from $\mathcal{N}_K(\mathbf{V} \mathbf{u}_i, \mathbf{V})$, where

$$\begin{cases} \mathbf{V} = (\mathbf{I}_K + \sigma_y^{-2} \boldsymbol{\theta} \boldsymbol{\theta}^\top + \sum_{m=1}^M \mathbf{\Lambda}_m^\top (\boldsymbol{\Gamma}_m \boldsymbol{\Gamma}_m^\top + \text{diag}(\sigma_m^2))^{-1} \mathbf{\Lambda}_m)^{-1} \\ \mathbf{u}_i = \sigma_y^{-2} \boldsymbol{\theta} (\mathbf{y}_i - \mu_y) + \sum_{m=1}^M \mathbf{\Lambda}_m^\top (\boldsymbol{\Gamma}_m \boldsymbol{\Gamma}_m^\top + \text{diag}(\sigma_m^2))^{-1} (\mathbf{z}_{mi} - \boldsymbol{\mu}_m) \end{cases}$$
5. for $i = 1, \dots, n$:
 - for $m = 1, \dots, M$:
 - sample $\boldsymbol{\phi}_{mi}$ from $\mathcal{N}_{K_m}(\mathbf{V}_m \mathbf{u}_{mi}, \mathbf{V}_m)$, where

$$\begin{cases} \mathbf{V}_m = (\mathbf{I}_{K_m} + \boldsymbol{\Gamma}_m^\top \text{diag}(\sigma_m^{-2}) \boldsymbol{\Gamma}_m)^{-1} \\ \mathbf{u}_{mi} = \boldsymbol{\Gamma}_m^\top \text{diag}(\sigma_m^{-2}) (\mathbf{z}_{mi} - \boldsymbol{\mu}_m - \mathbf{\Lambda}_m \boldsymbol{\eta}_i) \end{cases}$$
6. for $h = 1, \dots, K$:
 - sample the binary indicator δ_h according to equation (A1)
 - for $m = 1, \dots, M$:
 - for $h = 1, \dots, K$:
 - sample the categorical indicator δ_{mh} according to equation (A1)
 - for $h = 1, \dots, K_m$:
 - sample the categorical indicator ζ_{mh} according to equation (A1)
7. sample ξ from $\mathcal{Be}(a^{(\xi)} + \sum_{h=1}^K \mathbb{1}_{(\delta_h=0)}, b^{(\xi)} + \sum_{h=1}^K \mathbb{1}_{(\delta_h=1)})$
 - for $m = 1, \dots, M$:
 - for $h = 1, \dots, K-1$:
 - sample ρ_{mh} from $\mathcal{Be}(1 + \sum_{l=1}^K \mathbb{1}_{(\delta_l=h)}, \alpha_m^{(\Lambda)} + \sum_{l=1}^K \mathbb{1}_{(\delta_l>h)})$

for $h = 1, \dots, K_m - 1$:
 sample ν_{mh} from $\mathcal{Be}(1 + \sum_{l=1}^K \mathbb{1}_{(\delta_l=h)}, \alpha_m^{(\Gamma)} + \sum_{l=1}^K \mathbb{1}_{(\delta_l>h)})$
 8. for $h = 1, \dots, K$:
 if $(\delta_h = 1 \text{ and } \max_m \delta_{mh} > h)$ sample χ_h^2 from
 $\mathcal{InvGa}(a^{(\theta)} + 0.5, b^{(\theta)} + 0.5 \theta_h^2)$ else set $\chi_h^2 = \chi_\infty^2$
 for $m = 1, \dots, M$:
 for $h = 1, \dots, K$:
 if $(\delta_{mh} > h \text{ and } (\delta_h = 1 \text{ or } \max_{m' \neq m} \delta_{m'h} > h))$ sample χ_{mh}^2 from
 $\mathcal{InvGa}(a_m^{(\Lambda)} + 0.5 p_m, b_m^{(\Lambda)} + 0.5 \sum_{j=1}^{p_m} \Lambda_{mj}^2)$ else set $\chi_{mh}^2 = \chi_{m\infty}^2$
 for $h = 1, \dots, K_m$:
 if $\zeta_{mh} > h$ sample τ_{mh}^2 from $\mathcal{InvGa}(a_m^{(\Gamma)} + 0.5 p_m, b_m^{(\Gamma)} + 0.5 \sum_{j=1}^{p_m} \Gamma_{mj}^2)$
 else set $\tau_{mh}^2 = \tau_{m\infty}^2$

To complete the specification of the sampler, we provide here the details for the computation of the probability mass functions of the latent indicators from the CUSP constructions. In particular, we employ the same strategy of original contribution by Legramanti et al. (2020), sampling all latent indicators from the corresponding collapsed full conditionals after the marginalization of the loadings variances χ_h^2, χ_{mh}^2 and τ_{mh}^2

$$\begin{aligned}
 \mathbb{P}[\delta_h = s_h \mid \{\delta_{mh} = s_{mh}\}_m, \boldsymbol{\theta}_h, \{\boldsymbol{\Lambda}_{m \bullet h}\}_m, \xi] &= (1 - \xi)^{s_h} \cdot \xi^{s_h} \cdot \\
 &\quad \cdot f(\boldsymbol{\theta}_h \mid \delta_h = s_h, \{\delta_{mh} = s_{mh}\}_m) \prod_{m=1}^M f(\boldsymbol{\Lambda}_{m \bullet h} \mid \delta_h = s_h, \{\delta_{m'h} = s_{m'h}\}_{m'}) \\
 \mathbb{P}[\delta_{mh} = s_{mh} \mid \delta_h = s_h, \{\delta_{m'h} = s_{m'h}\}_{m' \neq m}, \boldsymbol{\theta}_h, \{\boldsymbol{\Lambda}_{m' \bullet h}\}_{m'}, \{\boldsymbol{\rho}_{m'}\}_{m'}] &= \xi_{m s_{mh}} \cdot \\
 &\quad \cdot f(\boldsymbol{\theta}_h \mid \delta_h = s_h, \{\delta_{m'h} = s_{m'h}\}_{m'}) \prod_{m'=1}^M f(\boldsymbol{\Lambda}_{m' \bullet h} \mid \delta_h = s_h, \{\delta_{m''h} = s_{m''h}\}_{m''}) \\
 \mathbb{P}[\zeta_{mh} = \ell_{mh} \mid \boldsymbol{\Gamma}_{m \bullet h}, \boldsymbol{\nu}_m] &= \omega_{m \ell_{mh}} \cdot f(\boldsymbol{\Gamma}_{m \bullet h} \mid \zeta_{mh} = \ell_{mh}),
 \end{aligned} \tag{A1}$$

where $s_h \in \{0, 1\}$, $s_{mh} \in \{1, \dots, K\}$ for each $m = 1, \dots, M$ and $h = 1, \dots, K$, while $\ell_{mh} \in \{1, \dots, K_m\}$ for each $m = 1, \dots, M$ and $h = 1, \dots, K_m$. Here we defined $\boldsymbol{\nu}_m = [\nu_{m1}, \dots, \nu_{mK_m}]^\top$ and $\boldsymbol{\rho}_m = [\rho_{m1}, \dots, \rho_{mK_m}]^\top$, while recall that $\xi_{mh} = \rho_{mh} \prod_{l=1}^{h-1} (1 - \rho_{ml})$ and $\omega_{mh} = \nu_{mh} \prod_{l=1}^{h-1} (1 - \nu_{ml})$. Similarly to Legramanti et al. (2020), the required loadings conditional pdf appearing in equation (A1) take the form

$$f(\boldsymbol{\Gamma}_{m \bullet h} \mid \zeta_{mh} = \ell_{mh}) = \begin{cases} t_{p_m, 2 a_m^{(\Gamma)}}(\boldsymbol{\Gamma}_{m \bullet h}; \mathbf{0}_{p_m}, (b_m^{(\Gamma)} / a_m^{(\Gamma)}) \mathbf{I}_{p_m}) & \text{if } \ell_{mh} > h \\ \phi_{p_m}(\boldsymbol{\Gamma}_{m \bullet h}; \mathbf{0}_{p_m}, \tau_{m\infty}^2 \mathbf{I}_{p_m}) & \text{otherwise} \end{cases}$$

and

$$\begin{aligned}
 f(\boldsymbol{\theta}_h \mid \delta_h = s_h, \{\delta_{mh} = s_{mh}\}_{m=1}^M) &= \\
 &\begin{cases} t_{2 a^{(\theta)}}(\boldsymbol{\theta}_h; \mathbf{0}, b^{(\theta)} / a^{(\theta)}) & \text{if } (s_h = 1 \text{ and } \max_m s_{mh} > h) \\ \phi(\boldsymbol{\theta}_h; \mathbf{0}, \chi_\infty^2) & \text{otherwise} \end{cases} \\
 f(\boldsymbol{\Lambda}_{m \bullet h} \mid \delta_h = s_h, \{\delta_{m'h} = s_{m'h}\}_{m'=1}^M) &= \\
 &\begin{cases} t_{p_m, 2 a_m^{(\Lambda)}}(\boldsymbol{\Lambda}_{m \bullet h}; \mathbf{0}_{p_m}, (b_m^{(\Lambda)} / a_m^{(\Lambda)}) \mathbf{I}_{p_m}) & \text{if } (s_{mh} > h \text{ and } (s_h = 1 \text{ or } \max_{m' \neq m} s_{m'h} > h)) \\ \phi_{p_m}(\boldsymbol{\Lambda}_{m \bullet h}; \mathbf{0}_{p_m}, \chi_{m\infty}^2 \mathbf{I}_{p_m}) & \text{otherwise,} \end{cases}
 \end{aligned}$$

where $t_{p, \kappa}(\cdot; \mathbf{r}, \mathbf{C})$ and $\phi_p(\cdot; \mathbf{r}, \mathbf{C})$ denotes the pdf of a p -variate Student- t and normal distributions, respectively, where $\kappa > 1$ stands for the degrees of freedom, \mathbf{r} is a location vector and \mathbf{C} is a scale matrix. As mentioned before, we consider a truncated version of the CUSP and D-CUSP priors, entailing finite upper bound K and $\{K_m\}_m$ to the number of shared and view-specific factors respectively. To preserve flexibility, we tune them adaptively according to Algorithm A2.

Algorithm A2: Adaption of the number of shared and view-specific factors at the t^{th} iteration of the Gibbs sampler.

```

 $u_t \sim \mathcal{U}(0, 1)$ 
if  $t \geq t_{adapt}$  and  $u_t < \exp(d_0 + d_1 t)$  then
     $K^* = K - \sum_{h=1}^K \mathbb{1}_{(\delta_h=1)} + \sum_{m=1}^M \mathbb{1}_{(\delta_{mh}>h)} \leq 1$ 
    if  $K^* < K - 1$  then
        set  $K = K^* + 1$ . Drop the inactive columns in  $\{\Lambda_m\}_m$  and  $\theta$ , along with the associated elements
        in  $\eta$ ,  $\{\chi_h\}_{h=1}^{K_m}$ ,  $\{\chi_{mh}\}_{h=1}^{K_m}$  and  $\{\xi_{mh}\}_{h=1}^{K_m}$ . Add an inactive shared factor, sampling from the spike
        the corresponding loadings and from the prior all other involved quantities
    else
        set  $K = K + 1$ . Add an inactive shared factor, sampling from the spike the corresponding
        loadings and from the prior all other involved quantities
    for  $m = 1, \dots, M$  do
         $K_m^* = K_m - \sum_{h=1}^{K_m} \mathbb{1}_{(\zeta_{mh} \leq h)}$ 
        if  $K_m^* < K_m - 1$  then
            set  $K_m = K_m^* + 1$ . Drop the inactive columns in  $\{\Gamma_m\}_m$ , along with the associated elements in
             $\phi_m$ ,  $\{\tau_{mh}\}_{h=1}^{K_m}$  and  $\{\omega_{mh}\}_{h=1}^{K_m}$ . Add an inactive specific factor for the  $m^{th}$  view, sampling
            from the spike the corresponding loadings and from the prior all other involved quantities
        else
            set  $K_m = K_m + 1$ . Add an inactive specific factor for the  $m^{th}$  view, sampling from the spike
            the corresponding loadings and from the prior all other involved quantities
    
```

Appendix B Modeling extensions for flexible data representations

Equation (1) can be viewed as the main building block of more complex modeling formulations, allowing greater flexibility in the descriptions of both the multiview data and the response component. In this section, we first address deviations from normality in the multiview data, which is a fragile assumption in Gaussian factor models. In many applications, such as multi-omics data, the features are often non-normally distributed, right-skewed, or present multi-modal marginals. Nonetheless, Gaussian formulations as in equations (1) demand that the latent factor decomposition simultaneously describe the dependence structure and the marginal distributions of the features. This can negatively affect the performance of the methodology, while having a confounding effect on the identification of latent sources of variation. To address this issue, we develop a copula factor model extension of JAFAR (Hoff 2007, Murray et al. 2013, Feldman & Kowal 2024), which allows us to disentangle learning of the dependence structure from that of margins. Notably, the D-CUSP prior structure described above readily applies to such extensions as well.

Furthermore, JAFAR can be easily generalized to account for deviations from normality and linearity in the response, other than binary and count y . Here we present different ways to achieve this, adapting the proposed D-CUSP prior. For the sake of completeness, we note that higher flexibility could be achieved also considering alternative approaches, beyond those reported below. For instance, recent contributions in factor models have shown the benefit of assuming a mixture of normals as prior distribution for the latent factors (Chandra, Canale & Dunson 2023).

B.1 Non-Gaussian data: single-view case & copula factor regression

For ease of exposition, we first introduce Copula Factor Models in the simplified case of a single set of features $\mathbf{x}_i \in \mathbb{R}^p$, before extending to the multiview case. Adhering to the formulation in (Hoff 2007), we model the joint distribution of \mathbf{x}_i as $F(\mathbf{x}_{i1}, \dots, \mathbf{x}_{ip}) = \mathcal{C}(F_1(\mathbf{x}_{i1}), \dots, F_p(\mathbf{x}_{ip}))$, where F_j is the univariate marginal distribution of the j^{th} entry, and $\mathcal{C}(\cdot)$ is a distribution function on $[0, 1]^p$ that describes the dependence between the variables. Any joint distribution F can be completely specified by its marginal distributions and a copula \mathcal{C} (Sklar 1959), with the copula being uniquely determined when the variables are continuous.

Here we employ the Gaussian Copula $\mathcal{C}(u_1, \dots, u_p) = \Phi_p(\Phi^{-1}(u_1), \dots, \Phi^{-1}(u_p) | \Sigma)$, where $\Phi_p(\cdot | \Sigma)$ is the p -dimensional Gaussian cdf with correlation matrix Σ , $\Phi(\cdot)$ is the univariate standard Gaussian cdf and $[u_1, \dots, u_p] \in [0, 1]^p$. Plugging in the Gaussian copula in the general formulation, the implied joint distribution of \mathbf{x}_i is

$$F(\mathbf{x}_{i1}, \dots, \mathbf{x}_{ip}) = \Phi_p\left(\Phi^{-1}(F_1(\mathbf{x}_{i1})), \dots, \Phi^{-1}(F_p(\mathbf{x}_{ip})) \mid \Sigma\right).$$

Hence, the Gaussian distribution is used to model the dependence structure, whereas the data have univariate marginal distributions $F_j(\cdot)$. The Gaussian copula model is conveniently rewritten via a latent variable representation, such that $\mathbf{x}_{ij} = F_j^{-1}(\Phi(\mathbf{z}_{ij}/c_j))$, with $\mathbf{z}_i \sim \mathcal{N}_p(\mathbf{0}_p, \Sigma)$. Here $F_j^{-1}(u) = \inf\{x : F_j(x) \geq u\}$, $\forall u \in (0, 1)$, is the pseudo-inverse of the univariate marginal of the j^{th} entry, \mathbf{z}_{ij} is the latent variable related to predictor j and observation i , and c_j is a positive normalizing constant. Following (Murray et al. 2013), the learning of the potentially large correlation structure Σ can proceed by endowing \mathbf{z}_i with a latent factor model $\mathbf{z}_i \sim \mathcal{N}_p(\Lambda \boldsymbol{\eta}_i, \mathbf{D})$, with $\mathbf{D} = \text{diag}(\{\sigma_j^2\}_{j=1}^p)$, $p \times k$ factor loadings matrix Λ and latent factors $\boldsymbol{\eta}_i \sim \mathcal{N}_K(\mathbf{0}_K, \mathbf{I}_K)$. Likewise, predictions of a continuous health outcome y_i can be accounted for via a regression on the latent factors $y_i \sim \mathcal{N}(f(\boldsymbol{\eta}_i), \sigma_y^2)$, where in JAFAR we consider a simple linear mapping $f(\boldsymbol{\eta}_i) = \boldsymbol{\theta}^\top \boldsymbol{\eta}_i$. In the latter case, the induced regression is linear also in \mathbf{z}_i :

$$\begin{aligned} \mathbb{E}[y_i \mid \mathbf{x}_i] &= \mathbb{E}[\boldsymbol{\theta}^\top \boldsymbol{\eta}_i \mid \mathbf{x}_i] = \boldsymbol{\theta}^\top \mathbb{E}[\boldsymbol{\eta}_i \mid \mathbf{x}_i] = \boldsymbol{\theta}^\top \mathbb{E}[\mathbb{E}[\boldsymbol{\eta}_i \mid \mathbf{z}_i] \mid \mathbf{x}_i] \\ &= \boldsymbol{\theta}^\top \mathbb{E}[(\Lambda^\top \mathbf{D}^{-1} \Lambda + \mathbf{I}_K)^{-1} \Lambda^\top \mathbf{D}^{-1} \mathbf{z}_i \mid \mathbf{x}_i] = \boldsymbol{\theta}^\top \mathbf{A} \mathbb{E}[\mathbf{z}_i \mid \mathbf{x}_i], \end{aligned}$$

where $\mathbb{E}[\mathbf{z}_i \mid \mathbf{x}_i]$ is a vector such that the j^{th} element is equal to $c_j \Phi^{-1}(F_j(\mathbf{x}_{ij}))$. This follows from the fact that the distribution of $\boldsymbol{\eta}_i \mid \mathbf{z}_i$ is normal with covariance $\mathbf{V} = (\Lambda^\top \mathbf{D}^{-1} \Lambda + \mathbf{I}_K)^{-1}$ and mean $\mathbf{A} \mathbf{z}_i$ where $\mathbf{A} = \mathbf{V} \Lambda^\top \mathbf{D}^{-1}$. To enforce standardization of the latent variables, $c_j = \sqrt{\sigma_j^2 + \sum_{h=1}^k \Lambda_{jh}^2}$, which would non-trivially complicate the sampling process. However, since the model is invariant to monotone transformations (Murray et al. 2013), we can use instead

$$\mathbf{x}_{ij} = F_j^{-1}(\Phi(\mathbf{z}_{ij})) \quad \mathbf{z}_i \sim \mathcal{N}_p(\Lambda \boldsymbol{\eta}_i, \mathbf{D}) \quad \boldsymbol{\eta}_i \sim \mathcal{N}(\mathbf{0}_K, \mathbf{I}_K).$$

The only element left to be addressed is the estimation of the marginal distributions F_j . In many practical scenarios, the features are continuous, or treated as such with negligible impact on the overall analysis. In such a setting, it is common to replace $F_j(\cdot)$ by the scaled empirical marginal cdf $\hat{F}_j(t) = \frac{n}{n+1} \sum_{i=1}^n \frac{1}{n} \mathbb{1}(\mathbf{x}_{ij} \leq t)$, benefiting from the associated theoretical properties (Klaassen et al. 1997). Alternatively, Hoff (2007) and Murray et al. (2013) viewed the marginals as nuisance parameters and targeted learning of the copula correlation for mixed data types via extended rank likelihood. Recently, Feldman & Kowal (2024) proposed an extension for fully Bayesian marginal distribution estimation, with remarkable computational efficiency for discrete data.

B.2 Non-Gaussian data: multiview case

Extending the same rationale to the multiview case, the copula factor model now targets the joint distribution of $\mathbf{x} = [\mathbf{x}_{1i}^\top, \dots, \mathbf{x}_{Mi}^\top]^\top$ as

$$F(\mathbf{x}_{1i}, \dots, \mathbf{x}_{Mi}) = \mathcal{C}(F_{11}(\mathbf{x}_{1i1}), \dots, F_{1p_1}(\mathbf{x}_{1ip_1}), \dots, F_{M1}(\mathbf{x}_{Mi1}), \dots, F_{Mp_M}(\mathbf{x}_{Mip_M})).$$

Here $p = \sum_{m=1}^M p_m$, while F_{mj} is the univariate marginal cdf of the j^{th} variable in the m^{th} view. The additive latent factor structure from equation (1) can be directly imposed on the transformed variables $\mathbf{z}_i = [\mathbf{z}_{1i}^\top, \dots, \mathbf{z}_{Mi}^\top]^\top$, introducing again the distinction between shared and view-specific factors. The overall model formulation becomes

$$\begin{aligned} \mathbf{x}_{mij} &= F_{mj}^{-1}(\Phi(\mathbf{z}_{mij})) \\ \mathbf{z}_{mi} &= \boldsymbol{\mu}_m + \Lambda_m \boldsymbol{\eta}_i + \Gamma_m \boldsymbol{\phi}_{mi} + \boldsymbol{\epsilon}_{mi} \\ y_i &= \mu_y + \beta^\top \mathbf{r}_i + \boldsymbol{\theta}^\top \boldsymbol{\eta}_i + e_i. \end{aligned} \tag{B1}$$

As before, F_{mj}^{-1} is the pseudo-inverse of F_{mj} . Missing data can be imputed by sampling the corresponding entries $\tilde{\mathbf{z}}_{mij} \sim \mathcal{N}(\boldsymbol{\mu}_m + \Lambda_{mj}^\top \boldsymbol{\eta}_i + \Gamma_{mj}^\top \boldsymbol{\phi}_{mi}, \sigma_{mj}^2)$ at each iteration of the sampler. When there is no direct interest in reconstructing the missing data, subject-wise marginalization of the missing entries can improve mixing compared to their imputation.

B.3 Non-linear response modeling: interactions & splines

The specific structure of JAFAR allows the introduction of a more flexible dependence of y_i on η_i with minimal computational drawbacks. While such non-linearity typically breaks down conditionally conjugate updates for the shared factor, all remaining components of the model are unaffected in this respect. Accordingly, the Gibbs sampler from the previous section remains unchanged, except for step 4. Analogous extensions of BSFP would instead require non-conjugate updates even for the view-specific factors, which would be highly detrimental to good mixing of the MCMC chain.

B.3.1 Interactions among latent factors

Aside from multiview integration frameworks, Ferrari & Dunson (2021) recently generalized Bayesian latent factor regression to accommodate interactions among the latent variables in the response component

$$y_i = \mu_y + \beta^\top \mathbf{r}_i + \theta^\top \eta_i + \eta_i^\top \Omega \eta_i + e_i,$$

where Ω is a $K \times K$ symmetric matrix. Other than providing theory on model misspecification and consistency, the authors showed that the above formulation induces a quadratic regression of y_i on the transformed concatenated features \mathbf{z}_i

$$\mathbb{E}[y_i | \mathbf{z}_i] = \mu_y + (\theta^\top \mathbf{A}) \mathbf{z}_i + \mathbf{z}_i^\top (\mathbf{A}^\top \Omega \mathbf{A}) \mathbf{z}_i + \text{tr}(\Omega \mathbf{V}), \quad (\text{B2})$$

where as before $\mathbf{V} = (\mathbf{A}^\top \mathbf{D}^{-1} \mathbf{A} + \mathbf{I}_K)^{-1}$ and $\mathbf{A} = \mathbf{V} \mathbf{A}^\top \mathbf{D}^{-1}$. The same results directly apply to JAFAR as well, as its composite nature is reflected solely in the structure of such matrices. In fact, recalling that here $\mathbf{A} = [\mathbf{A}_1^\top, \dots, \mathbf{A}_M^\top]^\top$, it is easy to show that now $\mathbf{D} = \text{block-diag}(\{\mathbf{D}_m\}_{m=1}^M)$, where $\mathbf{D}_m = \mathbf{\Gamma}_m \mathbf{\Gamma}_m^\top + \text{diag}(\sigma_m^2)$ represent the marginal covariance structure of the m^{th} view conditioned on the shared factors η_i , after marginalization of the specific ones ϕ_{mi} . Accordingly, the additive structure of JAFAR allows once again to cut down computations, as the bottleneck evaluation of $\mathbf{A}^\top \mathbf{D}^{-1} \mathbf{A} = \sum_{m=1}^M \mathbf{A}_m^\top \mathbf{D}_m^{-1} \mathbf{A}_m$ can be done at $\mathcal{O}(\sum_{m=1}^M p_m (K + K_m)^2)$ cost rather than $\mathcal{O}((\sum_{m=1}^M p_m)(K + \sum_{m=1}^M K_m)^2)$. Notice that, as in the original contribution by Ferrari & Dunson (2021), we could define Ω as a diagonal matrix and we would still estimate pairwise interactions between the regressors. In such case, the D-CUSP prior would unfold also each element Ω_{hh} , for instance setting

$$\Omega_{hh} \sim \mathcal{N}(0, \gamma_h^2) \quad \gamma_h^2 \sim \psi_h \text{InvGa}(a^{(\Omega)}, b^{(\Omega)}) + (1 - \psi_h) \delta_{\gamma_{\infty}^2}.$$

Through appropriate modifications of the factor modeling structure, the same rationale can be extended to accommodate higher-order interactions, or interactions among the shared factors η_i and the clinical covariates \mathbf{r}_i . Conversely, we highlight that the standard version of JAFAR would induce a linear regression of y_i on the feature data, which boils down to dropping the last two terms on the right of equation (B2). The inclusion of pairwise interactions among the factors in the response component breaks conditional conjugacy for the shared factors. To address this issue, the authors suggested updating η_i using the Metropolis-adjusted Langevin algorithm (MALA) (Grenander and Miller 1994; Roberts and Tweedie 1996). In this respect, we highlight that a similar quadratic extension of BSFP would require updating $(M + 1) \cdot n$ vectors, of dimensions $\{K, K_1, \dots, K_M\}$, while JAFAR allows to reduce this major computational bottleneck to n vectors of dimensions K .

B.3.2 Bayesian B-splines

To allow for higher flexibility of the response surface, one possibility is to model the continuous outcome with a nonparametric function of the latent variables. As this would however create several computational challenges, we instead focus on modeling $f(\cdot)$ using Bayesian B-splines of degree D :

$$f(\eta_i) = \sum_{h=1}^K \sum_{d=1}^{D+2} \Theta_{hd} b_d(\eta_{ih}),$$

where $b_d(\cdot)$, for $d = 1, \dots, D + 2$, denotes the d^{th} function in a B-spline basis of degree D with natural boundary constraints. Let $\varrho = (\varrho_1, \dots, \varrho_D)$ be the boundary knots, then $b_1(\cdot)$ and $b_{D+2}(\cdot)$ are linear functions

in the intervals $[-\infty, \varrho_1]$ and $[\varrho_D, +\infty]$, respectively. In particular, we assume cubic splines (i.e. $D = 3$), but the model can be easily estimated for higher-order splines. As before, the update of the shared factors needs to be performed via a Metropolis-within-Gibbs step, without modifying the other steps of the sampler. In such a case, the D-CUSP can be extended simply by setting

$$\Theta_{hd} \sim \mathcal{N}(0, \chi_h^2) \quad \chi_h^2 \sim \psi_h \text{Inv}\mathcal{G}a(a^{(\theta)}, b^{(\theta)}) + (1 - \psi_h) \delta_{\chi_\infty^2}.$$

B.4 Categorical and count outcomes: GLMs factor regression

The JAFAR construction can be modified to accommodate for non-continuous outcomes y_i as well, while still allowing for deviation from linearity assumptions via the quadratic regression setting presented above. For instance, binary responses can be trivially modeled via a probit link $y_i \sim \text{Ber}(\varphi_i)$ with $\varphi_i = \Phi(\theta^\top \boldsymbol{\eta}_i + \boldsymbol{\eta}_i^\top \boldsymbol{\Omega} \boldsymbol{\eta}_i)$. Except for the shared factors $\boldsymbol{\eta}_i$, conditional conjugacy is preserved by appealing to a well-known data augmentation strategy in terms of latent variable $q_i \in \mathbb{R}$ (Albert & Chib 1993), such that $y_i = 1$ if $q_i > 0$ and $y_i = 0$ if $q_i \leq 0$.

More generally, in the remainder of this section, we show how to extend the same rationale to generalized linear models (GLM) with logarithmic link and responses in the exponential families. In doing so, we also compute expressions for induced main and interaction effects, allowing for a straightforward interpretation of the associated coefficients.

B.4.1 Factor regression with count data

In GLMs under logarithmic link, the logarithmic function is used to relate the linear predictor $\boldsymbol{\beta}^\top \mathbf{r}_i$ to the conditional expectation of y_i given the covariates \mathbf{r}_i , such that $\log(\mathbb{E}[y_i | \mathbf{r}_i]) = \boldsymbol{\beta}^\top \mathbf{r}_i$. Two renowned GLMs for count data are the Poisson and the Negative-Binomial models. Defining φ_i as the mean parameter for the i^{th} observation $\varphi_i = \mathbb{E}[y_i | \mathbf{r}_i] = e^{\boldsymbol{\beta}^\top \mathbf{r}_i}$, such two alternatives correspond to $(y_i | \mathbf{r}_i) \sim \text{Poisson}(\varphi_i)$ and $(y_i | \mathbf{r}_i) \sim \text{NegBin}(\kappa/(\varphi_i + \kappa), \kappa)$, for some $\kappa \in [0, 1]$. A main limitation of the Poisson distribution is the fact that the mean and variance are equal, which motivates the use of negative-binomial regression to deal with over-dispersed count data. In both scenarios, we can integrate the GLM formulation in the quadratic latent factor structure presented above

$$\log(\mathbb{E}[y_i | \boldsymbol{\eta}_i]) = \boldsymbol{\theta}^\top \boldsymbol{\eta}_i + \boldsymbol{\eta}_i^\top \boldsymbol{\Omega} \boldsymbol{\eta}_i$$

Accordingly, it is easy to show the following.

Proposition 1 *Marginalizing out all latent factors in the quadratic GLM extension of JAFAR, both shared and view-specific ones, it holds that*

$$\mathbb{E}[y_i | \mathbf{z}_i] = \sqrt{|\mathbf{V}'|/|\mathbf{V}|} \exp\left(\frac{1}{2} \boldsymbol{\theta}^\top \mathbf{V}' \boldsymbol{\theta} + \boldsymbol{\theta}_X^\top \mathbf{z}_i + \mathbf{z}_i^\top \boldsymbol{\Omega}_X \mathbf{z}_i\right)$$

where $\boldsymbol{\theta}_X^\top = \boldsymbol{\theta}^\top (\mathbf{I}_K - 2\mathbf{V}\boldsymbol{\Omega})^{-1} \mathbf{A}$, $\boldsymbol{\Omega}_X = \frac{1}{2} \mathbf{A}^\top \mathbf{V}^{-1} ((\mathbf{I}_K - 2\mathbf{V}\boldsymbol{\Omega})^{-1} - \mathbf{I}_K) \mathbf{A}$ and $\mathbf{V}' = (\mathbf{V}^{-1} - 2\boldsymbol{\Omega})^{-1}$. As before, $\mathbf{V} = (\mathbf{A}^\top \mathbf{D}^{-1} \mathbf{A} + \mathbf{I}_K)^{-1}$ and $\mathbf{A} = \mathbf{V} \mathbf{A}^\top \mathbf{D}^{-1}$ comes for the full-conditional posterior of the shared factors $\boldsymbol{\eta}_i | \mathbf{z}_i \sim \mathcal{N}_K(\mathbf{A} \mathbf{z}_i, \mathbf{V})$, after marginalization of the view-specific factors.

This allows us to estimate quadratic effects with high-dimensional correlated predictors in regression settings with count data. Similarly to what seen before, the composite structure of JAFAR affects solely the bottleneck computation of the massive matrix $\mathbf{A}^\top \mathbf{D}^{-1} \mathbf{A}$, allowing to substantially reduce the associated computational cost by conveniently decomposing it.

B.4.2 Exponential family responses

We consider here an even more general scenario requiring only that the outcome distribution belongs to the exponential family

$$p(y_i | \varsigma_i) = \exp(\varsigma_i \cdot T(y_i) - U(\varsigma_i)),$$

where ς_i is the univariate natural parameter and $T(y_i)$ is a sufficient statistic. Accordingly, we generalize Gaussian linear factor models and set $\varsigma_i = \boldsymbol{\theta}^\top \boldsymbol{\eta}_i + \boldsymbol{\eta}_i^\top \boldsymbol{\Omega} \boldsymbol{\eta}_i$. As before, $\varphi_i = \mathbb{E}[y_i | \boldsymbol{\eta}_i] = g^{-1}(\boldsymbol{\theta}^\top \boldsymbol{\eta}_i + \boldsymbol{\eta}_i^\top \boldsymbol{\Omega} \boldsymbol{\eta}_i)$,

where $g(\cdot)$ is a model-specific link function. Our goal is to compute the expectation of y_i given \mathbf{z}_i after integrating out all latent factors

$$\begin{aligned}\mathbb{E}[y_i|\mathbf{z}_i] &= \mathbb{E}[\mathbb{E}[y_i|\boldsymbol{\eta}_i]|\mathbf{z}_i] = \mathbb{E}[g^{-1}(\boldsymbol{\theta}^\top \boldsymbol{\eta}_i + \boldsymbol{\eta}_i^\top \boldsymbol{\Omega} \boldsymbol{\eta}_i)|\mathbf{z}_i] \\ &= \int g^{-1}(\boldsymbol{\theta}^\top \boldsymbol{\eta}_i + \boldsymbol{\eta}_i^\top \boldsymbol{\Omega} \boldsymbol{\eta}_i) p(\boldsymbol{\eta}_i|\mathbf{z}_i) d\boldsymbol{\eta}_i.\end{aligned}$$

In general, this represents the expectation of the natural parameter conditional on \mathbf{z}_i for any distribution within the exponential family. Endowing the stacked transformed features \mathbf{z}_i with the additive factor model above, i.e. $\mathbf{z}_{mi} \sim \mathcal{N}_{p_m}(\boldsymbol{\mu}_m + \boldsymbol{\Lambda}_m \boldsymbol{\eta}_i, \boldsymbol{\Gamma}_m \boldsymbol{\Gamma}_m^\top + \text{diag}(\boldsymbol{\sigma}_m^2))$, we have that $p(\boldsymbol{\eta}_i|\mathbf{z}_i)$ is pdf of a normal distribution with mean $\mathbf{A} \mathbf{z}_i$ and variance \mathbf{V} (see Proposition 1). In this case, the above integral can be solved when $g^{-1}(\cdot)$ is the identity function, as in linear regression, or the exponential function, as in regression for count data or survival analysis. On the contrary, when we are dealing with a binary regression and $g^{-1}(\cdot)$ is equal to the logit, the above integral does not have an analytical solution. However, recalling that in such case φ_i represents the probability of success, we can integrate out the latent variables and compute the expectation of the log-odds conditional on \mathbf{z}_i

$$\mathbb{E}\left[\log\left(\frac{\varphi_i}{1-\varphi_i}\right) \middle| \mathbf{z}_i\right] = \mathbb{E}[\boldsymbol{\theta}^\top \boldsymbol{\eta}_i + \boldsymbol{\eta}_i^\top \boldsymbol{\Omega} \boldsymbol{\eta}_i|\mathbf{z}_i] = (\boldsymbol{\theta}^\top \mathbf{A}) \mathbf{z}_i + \mathbf{z}_i^\top (\mathbf{A}^\top \boldsymbol{\Omega} \mathbf{A}) \mathbf{z}_i + \text{tr}(\boldsymbol{\Omega} \mathbf{V}).$$

Appendix C Generating Realistic Loadings Matrices

In the current section, we describe an original way to generate loading matrices inducing realistic block-structured correlations. This represents a significant improvement in targeting realistic simulated data, compared to many studies in the literature. Focusing on a single loading matrix $\boldsymbol{\Lambda} \in \mathbb{R}^{p \times K}$ for ease of notation, Ding et al. (2022) set $\boldsymbol{\Lambda} = [\mathbf{I}_K, \mathbf{0}_{K \times (p-K)}]^\top$, which gives $\boldsymbol{\Lambda} \boldsymbol{\Lambda}^\top = \text{block-diag}(\{\mathbf{I}_K, \mathbf{0}_{K \times (p-K)}\})$. Samorodnitsky et al. (2024) samples independently $\boldsymbol{\Lambda}_{jh} \sim \mathcal{N}(0, 1)$, so that $\mathbb{E}[(\boldsymbol{\Lambda} \boldsymbol{\Lambda}^\top)_{jj'}] = \delta_{j,j'} \cdot K$. Poworoznek et al. (2021) enforce a simple sparsity pattern in the loadings, dividing the p features into K groups and sampling $\boldsymbol{\Lambda}_{jh} \sim \delta_{g(j),h} \mathcal{N}(0, v_{slab}^2) + (1 - \delta_{g(j),h}) \mathcal{N}(0, v_{spike}^2)$, for some $v_{slab}^2 \gg v_{spike}^2$ and representing by $g(j)$ the group assignment. This still gives $\mathbb{E}[(\boldsymbol{\Lambda} \boldsymbol{\Lambda}^\top)_{jj'}] = \delta_{j,j'} \cdot (v_{slab}^2 + (K-1) \cdot v_{spike}^2)$. Although the generation of a specific loading matrix entails single samples rather than expectations, the induced correlation matrices are not expected to present any meaningful structure.

To overcome this issue, we further leverage the grouping of the features, allowing each group to load on multiple latent factors and centering the entries of each group around some common hyper-loading μ_g , for $g = 1, \dots, G$. To induce blocks of positive and negatively correlated features, we propose setting $\mu_g = (-1)^g \tilde{\mu}_g$, with $\tilde{\mu}_g$ sampled from a density f_+ with support on the positive real line. Our default suggestion is to set f_+ to be a beta distribution $\mathcal{Be}(5, 3)$. Conditioned on such hyper-loadings and the group assignments, we sample the loading entries independently from $\boldsymbol{\Lambda}_{jh} \sim \mathcal{N}(\mu_{g(j)}/\sqrt{K}, v_o^2/K)$, resulting in $\mathbb{E}[(\boldsymbol{\Lambda} \boldsymbol{\Lambda}^\top)_{jj'}] = (-1)^{g(j)} (-1)^{g(j')} \tilde{\mu}_{g(j)} \tilde{\mu}_{g(j')} + \delta_{j,j'} v_o^2$. This naturally translates into blocks of features with correlations of alternating signs and different magnitudes. The core structure above can be complemented with further nuances, to recreate more realistic patterns. This includes group-wise sign permutation, introducing entry-wise and group-wise sparsity, and the addition of a layer of noise loadings $\mathcal{N}(0, r_{damp} v_o^2/K)$ to avoid exact zeros.

In our simulation studies from Section 3, we set $v_o^2 = 0.1$ and $r_{damp} = 1e^{-2}$. Finally, view-wise sparsity can be imposed on the shared loadings of the JAFAR structure to achieve composite activity patterns in the respective component of the model. The resulting generation procedure for a view-specific loading matrix is summarized in Algorithm C1.

Appendix D Simulated data: further results

In the present section, we provide further evidence of the performances of the proposed methodology on the simulated data. We begin by complementing the results from Figure 2 with the associated uncertainty

Algorithm C1: Generation of Realistic Loading Matrices.

```

 $\Lambda = \mathbf{0}_{p \times K}$ 
for  $g = 1, \dots, G$  do
     $\tilde{\mu}_g \sim f_+$ 
     $\mu_g = (-1)^g \tilde{\mu}_g$ 
    for  $h = 1, \dots, K$  do
         $u_{gh} \sim \text{Bern}(\pi^{(g)})$ 
         $s_{gh} \sim \text{Bern}(\pi^{(s)})$ 
for  $j = 1, \dots, p$  do
     $g(j) \sim \text{Cat}_G(\{\pi_g\}_{g=1}^G)$ 
    for  $h = 1, \dots, K$  do
         $r_{jh} \sim \text{Bern}(\pi^{(e)})$ 
         $\ell_{jh}^{(1)} \sim \mathcal{N}(\mu_g / \sqrt{K}, v_o^2 / K)$ 
         $\ell_{jh}^{(o)} \sim \mathcal{N}(0, r_{\text{damp}} v_o^2 / K)$ 
         $\Lambda_{jh} = u_{g(j)h} \cdot (2s_{g(j)h} - 1) \cdot r_{jh} \cdot \ell_{jh}^{(1)} + \ell_{jh}^{(o)}$ 
    
```

[hyper-loadings magnitude]

[signed hyper-loadings]

[group-wise sparsity]

[group-wise sign switch]

[group assignment]

[entry-wise sparsity]

[main signal]

[spurious signal]

[composite signal]

Return Λ

quantification. Figure D1 shows that that all considered methods achieve similar performances, incurring under-coverage and over-coverage in the train and test sets, respectively.

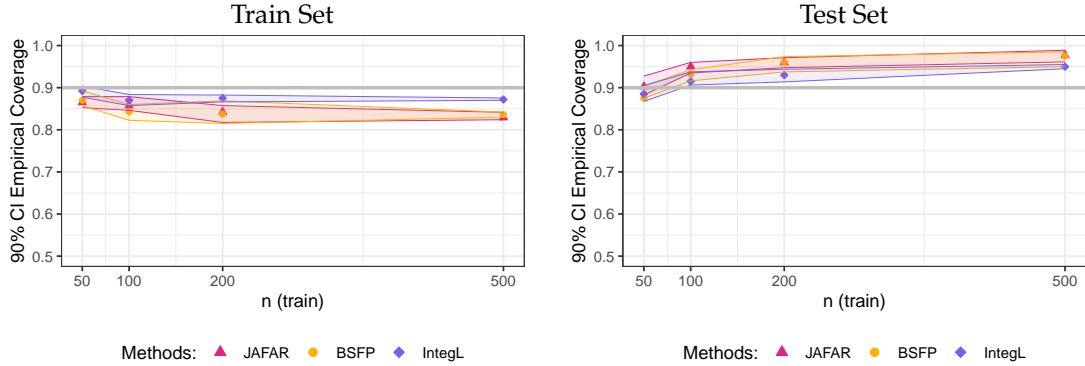


Figure D1: Empirical coverage of the 90% predictive intervals on the train sets (left) and test sets (right) of simulated data. The x-axis reports increasing size of the train set. The interior points and band edges correspond to the quartiles over 10 independent replicates for fixed dimensions. The horizontal gray lines correspond to the correct coverage.

To provide more insight into feature structure learning, we further break down the results for one of the replicates for $n = 500$ from Section 3. We focus first on induced coefficients $\beta_m = \beta_m(\Lambda_m, \Gamma_m, \sigma_m^2, \theta)$ in the induced linear regression $\mathbb{E}[y_i | \{\mathbf{X}_{mi}\}_{m=1}^M] = \sum_{m=1}^M \beta_m \mathbf{X}_{mi}$. Recall that we set up the simulations so that half of the features of each view do not load directly to response-related factors. This translates into small values of the associated regression coefficients, while collinearity with other features prevents them from being exactly zero. The results in Figure D2 show the capability of JAFAR to distinguish which features are more relevant for predictive purposes.

Finally, in Figure D3, we report the correlation matrices for each view, conditioned on all the others. For the two-factor models, we obtained the latter from the empirical correlations computed on independent samples from $p(\mathbf{X}_m | \{\mathbf{X}_{m'}\}_{m' \neq m})$, where JAFAR still achieves superior predictors reconstruction.

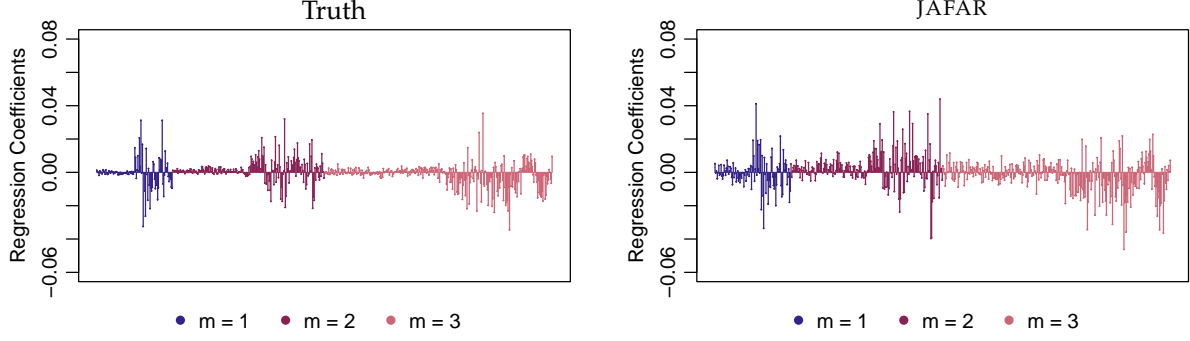


Figure D2: Regression coefficients in one replicate of the considered simulated data for $n = 500$. For JAFAR, these corresponded to the Monte Carlo average of the induced coefficients. JAFAR manages to distinguish between weakly and strongly predictive features.

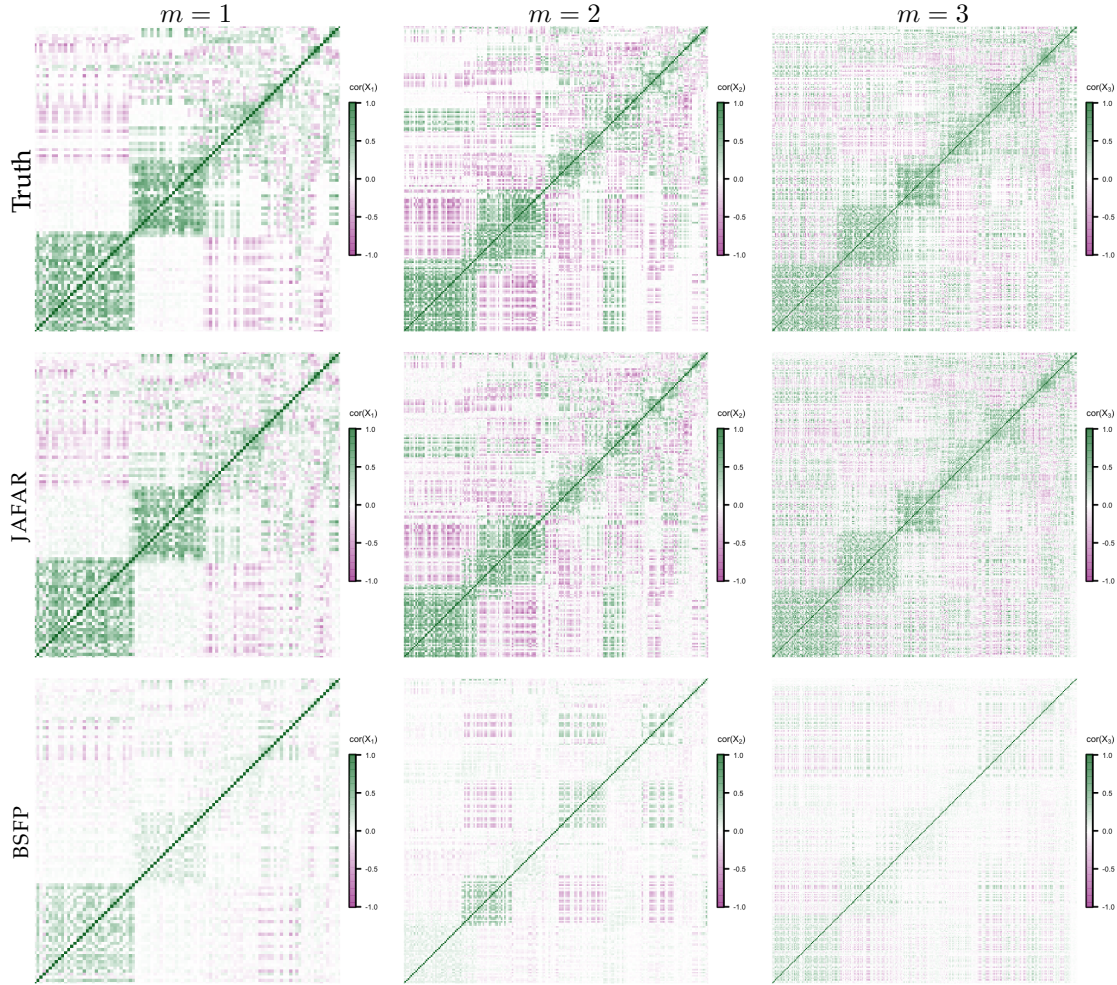


Figure D3: Within-view correlation matrices in one replicate of the considered simulated data for $n = 500$. The first row reports the true correlations for each view, conditioned on the remaining ones. The realistic block structure is obtained via our original simulation setup for the loading matrices, detailed in Appendix C. For JAFAR and BSFP, we considered here the average correlations matrix $\frac{1}{n_{\text{MCMC}}} \sum_{t=1}^{n_{\text{MCMC}}} \text{cor}(\mathbf{X}_m^{(t)})$ over MCMC samples from the full conditional $\mathbf{X}_m^{(t)} \sim p(\mathbf{X}_m \mid \{\mathbf{X}_{m'}\}_{m' \neq m})$ of the corresponding view given all the others (response excluded).

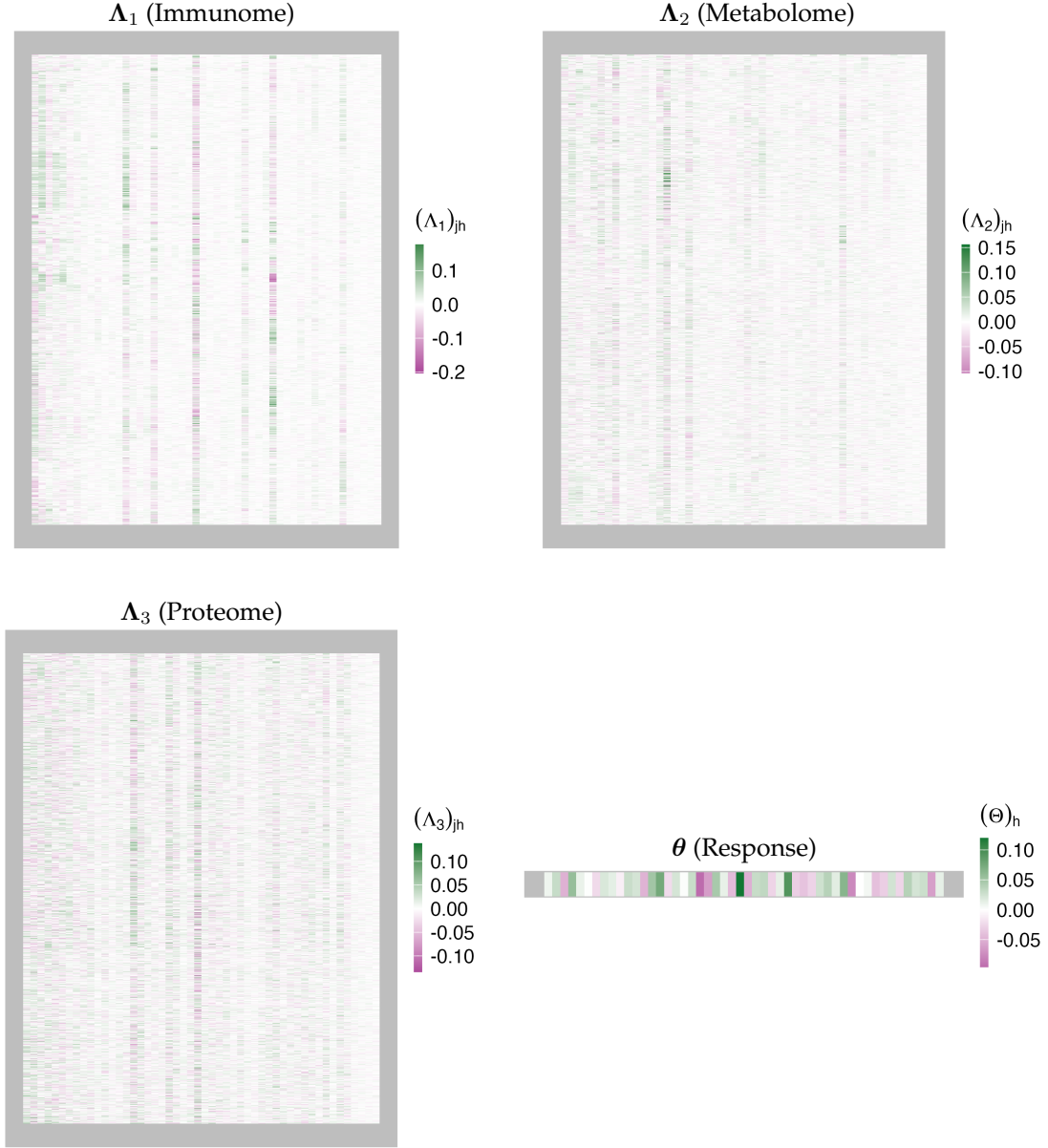


Figure E4: Posterior means of the shared-component loadings matrices, after post-processing via multiview Varimax.

Appendix E Labor onset prediction: further results

In the present section, we provide further evidence of the performances of the proposed methodology on the application from Section 4. In Figure E4, we report the posterior mean of the shared loading matrices after postprocessing using the extended version of MatchAlign via Multiview Varimax.

In the left panel of Figure E5, we report the induced coefficients for the regression directly tackling $p(y_i | \{\mathbf{X}_{mi}\}_{m=1}^M, -)$, i.e. marginalizing out all latent factors. This supports the evidence that all omics layers bear predictive power. In the right panel, we also summarize the squared error of JAFAR in predicting the response in the test set when holding out one entire omics layer at a time, indicating only a moderate effect on prediction accuracy. This suggests that the corresponding joint latent sources of variation capture underlying biological processes that affect the system as a whole.

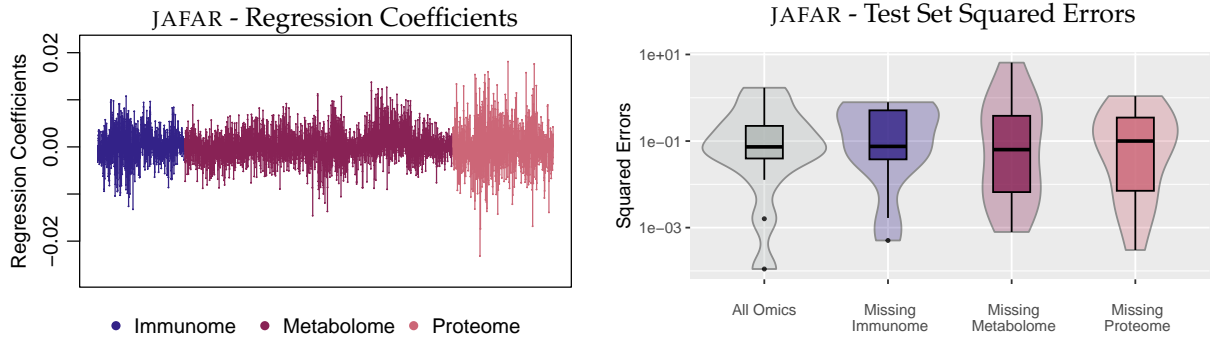


Figure E5: Induced linear regression coefficients for the response y_i on the omics data $\{\mathbf{x}_{mi}\}_m$ (left). The reported values correspond to the average over the MCMC chain. All three omics layers appear to be significant for prediction purposes, as confirmed by the leave-one-omics-out predictive squared errors (right). Prediction under an entirely missing omics layer is a straightforward task in factor models.